2020

EXPERIMENTAL CHARACTERIZATION OF SPOOL VALVE FLOW NOISE

Zachary Cohen
Michigan Technological University, zjcohen@mtu.edu

EXPERIMENTAL CHARACTERIZATION OF SPOOL VALVE FLOW NOISE

By

Zachary J.V. Cohen

A THESIS

Submitted in partial fulfillment of the requirements for the degree of

MASTER OF SCIENCE

In Mechanical Engineering

MICHIGAN TECHNOLOGICAL UNIVERSITY

2020

This thesis has been approved in partial fulfillment of the requirements for the Degree of MASTER OF SCIENCE in Mechanical Engineering.

Department of Mechanical Engineering

Thesis Co-advisor: *Dr. Andrew Barnard*

Thesis Co-advisor: *Dr. Sriram Malladi*

Committee Member: *Dr. Yongchao Yang*

Department Chair: *Dr. William Predebon*

Contents

List of Figures . . . . . **ix**

List of Tables . . . . . **xiii**

Acknowledgments . . . . . **xv**

Abstract . . . . . **xvii**

1 Introduction **1**

1.1 Motivation 2

1.2 Objective 3

2 Theory of Hydraulic Flow Noise and Noise Mechanisms **5**

2.1 Noise Mechanisms in Hydraulic Circuits 5

2.1.1 Flow Generated Noise 7

2.1.1.1 Cavitation 7

2.1.1.2 Impact 9

2.1.1.3 Instability 10

2.1.1.4 Flow Noise 11

2.2 Reynolds Number 14

2.3 Froude Number 15

3 Methods and Materials 17

3.1 Valve Test Bench Development 18

3.2 Construction of Valve Circuit 20

3.2.1 Construction of Orifice Circuit 22

3.3 Simple Orifice Assumption Comparison 26

3.3.1 Valve Area Sweep Test Procedure 27

3.4 Data Processing 28

3.4.1 Instrumentation 31

3.5 Test Bench Operation 34

3.5.1 Test Bench Safety 36

3.6 Summary 36

4 Results 37

4.1 Needle Valve Flow Noise 38

4.2 Expansion Chamber Flow Noise Results 42

4.3 4 Meter Hose Flow Noise Results 43

4.4 Flow Noise Dependence on Static Variables 44

4.5 Combined Results 46

4.6 Summary 49

5 Conclusions **51**

References **55**

A Test Configuration Component List **59**

A.1 Spool Valve 59

B Additional Figures **63**

C Test Bench Startup Procedure **75**

D Removal of Electrical Noise from Dynamic Pressure Sensor Signals **77**

List of Figures

3.1 2.13 m Hose Hydraulic Test Circuit for Mount Energy Loss Tests . 18

3.2 Modified Hydraulic Test Bench Circuit with Spool Valve 19

3.3 Spool Valve Test Bench Schematic 21

3.4 Orifice Test Bench Schematic 23

3.5 Closeup view of needle valve boundary condition being tested on orifice 24

3.6 Closeup of Expansion Chamber Installed on Orifice. 24

3.7 View of 4 Meter Hose Installed on Orifice. 25

3.8 Orifice Housing and Pressure Sensor Locations on Adapters 26

3.9 50% Overlap Data Sampling Structure 29

3.10 Visualization of Orifice Data Matrix Structure for a Single Boundary Condition 30

3.11 Transducer Locations on Spool Valve 32

3.12 Static Pressure Sensor Location 33

3.13 Tachometer Orientation on Motor Pump Coupling Showing Safety Cage 34

3.14 Valve Circuit Wiring Diagram 35

4.1 (Top) Needle Valve Boundary Condition - Valve Spectra With and Without Harmonics Filtered Out - 1000 PSI 2000 RPM. (Bottom) Time series of normalized cross section area vs. normalized pressure comparing valve and orifices showing difference in amplitude for smallest orifice size. 38

4.2 Spectra at Inlet and Outlet for 3.50 mm (Top) showing strong cavitation on outlet sensor, 5.02 mm (Mid) and 8.06 mm (Bottom) Do Not Produce Cavitation- 1000 PSI, 2000 RPM 39

4.3 (Top) Needle Valve Boundary Condition - Dynamic Pressure Spectra at Valve Outlet - 1500psi - 1000rpm (Bottom) Agreement Between Smallest Orifice and Valve for Higher Back Pressure and Slower Motor Speed 40

4.4 Spectra at Outlet for 3.50 mm (Top), 5.02 mm (Mid) and 8.06 mm (Bottom) Overlaid with Valve Showing Similar Autopower Spectrum - 1500 PSI, 1000 RPM 41

4.5 Flow Noise as a Function of Cross Section Area and Static Pressure for 2000 RPM Test - Needle Valve Boundary Condition. 41

4.6 Flow Noise vs. Cross Section Area - 1000 psi 1000 rpm - Expansion Chamber 42

4.7 Divergence in Valve and Orifice Flow Noise - 2000 psi 2000 rpm - Expansion Chamber 43

4.8 Flow Noise vs. Cross Section Area with Difference in Small Orifice Amplitude Due to Cavitation - 2000 psi 2000 rpm - 4 Meter Hose . 44

4.9 Evolution of Volume Flow Rate and Static Pressure for 1000 psi and 1500 psi - 1000 RPM Tested on Needle Valve. 45

4.10 Normalized Flow Noise Amplitude vs. Static Pressure for 1000 psi and 1500 psi at 1000 RPM Tested on Needle Valve. 46

4.11 Full Flow Noise Data Set Showing Distinct Clusters Based on Volume Flow Rate 47

4.12 Full Flow Noise Data Set Normalized by Volume Flow Rate 48

4.13 Froude Number vs Normalized Flow Noise with Region Curve Fits for All Boundary Conditions. 49

B.1 Flow Noise - Expansion Chamber - 1000 psi 1000 rpm 64

B.2 Flow Noise - Expansion Chamber - 1000 psi 1500 rpm 64

B.3 Flow Noise - Expansion Chamber - 1000 psi 2000 rpm 65

B.4 Flow Noise - Expansion Chamber - 2000 psi 1500 rpm 65

B.5 Flow Noise - Expansion Chamber - 2000 psi 2000 rpm 66

B.6 Flow Noise - 4 Meter Hose - 1000 psi 1000 rpm 66

B.7 Flow Noise - 4 Meter Hose - 1000 psi 1500 rpm 67

B.8 Flow Noise - 4 Meter Hose - 1000 psi 2000 rpm 67

B.9 Flow Noise - 4 Meter Hose - 2000 psi 1500 rpm 68

B.10 Flow Noise - 4 Meter Hose - 2000 psi 2000 rpm 68

B.11 Flow Noise - Needle Valve - 500 psi 1000 rpm 69

B.12 Flow Noise - Needle Valve - 1000 psi 1000 rpm 69

B.13 Flow Noise - Needle Valve - 1500 psi 1000 rpm 70

B.14 Flow Noise - Needle Valve - 500 psi 1500 rpm 70

B.15 Flow Noise - Needle Valve - 1000 psi 1500 rpm 71

B.16 Flow Noise - Needle Valve - 1500 psi 1500 rpm 71

B.17 Flow Noise - Needle Valve - 500 psi 2000 rpm 72

B.18 Flow Noise - Needle Valve - 1000 psi 2000 rpm 72

B.19 Flow Noise - Needle Valve - 1500 psi 2000 rpm 73

D.1 Electrical Noise Corruption of Dynamic Pressure Sensor Signal and Smoothed Results 78

List of Tables

3.1 Test Bench Requirements 19

3.2 Hydraulic Oil Specifications 20

3.3 Spool Valve Test Bench Primary Component List 22

3.4 Three Boundary Condition Specifications 28

4.1 Coefficients from Curve Fitting and Corresponding R^2 Values . . . 49

A.1 Spool Valve Configuration Component List 60

A.2 Instrumentation Component List 61

Acknowledgments

Sincere thanks go to my advisors, Dr. Andrew Barnard and Dr. Sriram Malladi, for their confidence in me completing this work, their tireless help throughout this project, and their support and guidance throughout my graduate experience as a whole. This research would not be possible without the knowledge and expertise provided by Joe Bobchik, Brendan Clark, Pravin Sondkar, Rich Romick and Sarah Young. Additional thanks go to Mike Johnson and Caterpillar Inc. and its Integrated Components and Solutions division for their funding and support throughout the project. Lastly, I want to thank all my family and friends who have loved and encouraged me.

Abstract

The purpose of this research was to experimentally measure the flow noise produced by a spool valve and compare with measurements of orifice flow noise to reduce flow noise modelling complexity. The similarities and differences are compared over a range of volume flow rates, back pressures, and cross section areas. The impact of down stream boundary conditions on the flow noise are also examined. The results are generalized and plotted against Froude number. The valve results are curve fit to generate empirical equations that can be used to predict flow noise under typical operating conditions. The valve and orifice data sets converge in certain regions, and conclusions are drawn for when valve flow noise can be modelled as orifice flow noise in the hydraulic circuit design stage.

Chapter 1

Introduction

Noise produced by hydraulic systems is a serious problem for off-highway equipment due to strong workplace noise level regulations as well as concerns for operator safety. Hydraulic noise is best treated at the design stage, but this requires knowledge of the how noise is produced. Typically a computational model can provide such knowledge. However, there is a need for experimental validation of these models. Another form of model is an empirical model which is derived from experimental data.

1.1 Motivation

Hydraulic systems are used because of their efficient power transfer to machine components. The demand for more powerful hydraulic systems comes with the drawback of increased noise and vibrations. Periodic fluctuations in flow and pressure produce fluid-borne noise (FBN) which interacts with hose walls and produces structure-borne noise (SBN). If this excitation occurs at or near the natural frequencies of the hose, significant vibration issues may lead to quickened fatigue failure of components. The noise associated with hydraulic components may also push total noise to harmful levels, which is strongly regulated in construction environments.

Valves allow an operator to direct hydraulic power to machine components. Valves can change the existing FBN produced by the pump or they can create new sound through impact, instability and cavitation [1]. The boundary condition of the valve inlet and outlet can cause reflections of the pressure ripple that change the FBN characteristics. These effects differ depending on the valve spool position.

Hydraulic circuits are complex and operate with a wide range of conditions. Software capable of modelling FBN exist and are used by test and validation engineers to design quieter hydraulic circuits. There is a need to experimentally characterize hydraulic components for comparison against simulations and equations to improve

the empirical models used.

A spool valve contains a complex internal geometry. When designing hydraulic circuits to work quietly, the engineer is faced with a challenging problem of representing the flow noise generated by the complex spool valve system. If assumptions are made that the spool valve generates flow noise similar to that produced by a simple orifice, model complexity is reduced and the design stage accelerated. This work aims to show when and how orifice generated flow noise can be used in place of the valve flow noise through experimental results.

1.2 Objective

The primary goals for the project are as follows:

- Experimentally measure flow noise produced by a spool valve and set of orifices.
- Develop an empirical model for the flow noise produced by the spool valve and set of orifices.
- Determine when the flow noise generated by the spool valve can be modelled by the orifice flow noise.

The ideal empirical model should account for:

1. Volume Flow Rate

2. Static Pressure

3. Cross Section Area

4. Downstream Boundary Conditions

Chapter 2

Theory of Hydraulic Flow Noise and Noise Mechanisms

Background information on the primary noise mechanisms in fluids are discussed with an emphasis on turbulent flow noise mechanisms.

2.1 Noise Mechanisms in Hydraulic Circuits

Fluid-borne noise is the main source of noise in hydraulic circuits. Pumps produce significant FBN as they work to periodically pressurize and expel hydraulic fluid into the circuit. Imperfect pump timings and over-pressurization produces flow ripple and

pressure ripple that propagate through the circuit superimposed on the mean fluid flow and pressure. This FBN interacts with the hose walls and produces strong SBN if the FBN occurs at or near the natural frequencies of the hose. Kolb [2] experimentally showed this FBN to SBN exchange occurs strongest at antinodes of fluid mode shapes excited by pumping harmonics.

FBN is calculated by

$$FBN = Q_{ripple} \cdot P_{ripple} \tag{2.1}$$

where Q_{ripple} and P_{ripple} are the dynamic components of the flow and pressure, respectively. SBN is calculated by

$$SBN = F_{dynamic} \cdot v_{dynamic} \tag{2.2}$$

where $F_{dynamic}$ and $v_{dynamic}$ are the dynamic force and dynamic velocity, respectively. The pump source impedance and flow ripple were previously characterized using ISO 10767-1:2015 [3] for the pump installed on the MTU test bench.

2.1.1 Flow Generated Noise

Spool valves operate by moving a spool to open and close the flow path. This valve design is more stable than a poppet valve. Valves are often modelled as a simple orifice (contraction) followed by the post-valve expansion. Valves change existing FBN characteristics by reflecting pressure ripple waves and altering the flow ripple as the incompressible fluid is subjected to expansions and contractions [4]. Valves can also produce new FBN through several methods discussed later.

Fluid-borne noise is often the main component of noise in hydraulic circuits. While much of the FBN is produced by the pump, valves can also produce FBN through cavitation, impact, instability [1] and turbulent flow noise. Cavitation is the worst contributor to FBN based on the potential for high sound levels and structural damage.

2.1.1.1 Cavitation

Cavitation occurs when the pressure of the fluid drops below that fluid's vapor pressure. As the fluid starts to boil, gas bubbles form and travel with the fluid. This typically occurs in or just downstream of a valve or other flow restriction because of the pressure drop that occurs from a restriction. The noise associated with cavitation

is the bursting of these bubbles.

The sound of cavitation is described as boiling or gravelly. It is loud enough to be detrimental to the sound quality of a machine. Cavitation can also result in mechanical damage to the hydraulic circuit [5]. Cavitation damage has been studied deeply for close to a century. Sreedhar et al's.[5] review discusses cavitation induced damage in detail.

When the bubbles implode downstream, they produce a shock wave that adds to the FBN. If this implosion occurs at or near hose boundaries, it can break away parts of the walls. This will pollute the hydraulic oil with debris and damage the pump and it will cause faster fatigue failure. Cavitation can and should be mitigated by ensuring the pressure drop is not low enough to allow the formation of entrapped gas bubbles in the hydraulic fluid.

In this work, care was taken to avoid cavitation. However, this was not always possible and some tests show significantly high amplitude noise due to cavitation. Cavitation depends on the pressure drop through the restriction as well as the fluid velocity. The likelihood of cavitation is calculated by the dimensionless cavitation factor σ according to Equation 2.3.

$$\sigma = \frac{[p - p_v]}{\frac{1}{2}\rho U^2} \tag{2.3}$$

Where p is the local pressure, p_v the fluid vapor pressure, ρ the fluid density and U the fluid velocity. Cavitation inception occurs at a critical cavitation factor where $\sigma_i = -C_{p,min}$ which is defined by

$$C_{p,min} = \frac{p_{min} - p_1}{\frac{1}{2}\rho U^2} \tag{2.4}$$

here p_{min} and p_1 are the minimum pressure in the flow and the inlet pressure, respectively. This is known as the coefficient of pressure. $C_{p,min}$ is a property of the geometry of the component the fluid is flowing through and the Reynolds number corresponding to the flow through the component. The minimum pressure does not always need to be less than or equal to the liquid's vapor pressure for cavitation to occur. The occurrence of cavitation can also be highly driven by the geometry of the restriction, according to Yan and Thorpe [6] and cavitation may occur at pressures much higher than the vapor pressure.

Where p_{min} and p_1 are the minimum pressure in the flow and the inlet pressure, respectively.

2.1.1.2 Impact

Fluid impacts, or water hammer, occur when fluid momentum changes suddenly, such as when a valve port is rapidly closed. Water hammer is a transient behavior and

is thus less concerning in a sound quality assessment. However, a strong impact can cause significant damage to pipe components and loosen fittings at pipe connections or mounting points. Ways of mitigating water hammer involve slowing the fluid velocity, lengthening the time over which a valve is changed, or slowing pressure wave velocity [7]. Water hammer can also be mitigated by using inline shock arrestors which act to dampen the pressure spike.

Water hammer is currently out of the scope of this project as it is more likely to occur with longer lengths of hose and improper valve operation. For all tests that will be run, the valve will be opened and closed slowly to avoid transient events like water hammer.

2.1.1.3 Instability

Valves that rely on a spring to depress the plug can be unstable. When the fluid reaches a pressure such that the force exerted on the plug face is greater than the spring force, the plug is lifted and fluid flows through this opening. Since the valve is open, the pressure of the fluid does not increase further.

While unseated, the spring-plug may be unstable and self-oscillate. This is more typical for poppet valves but can occur in spool valves as well [1]. This oscillation produces a single frequency tone, which can be especially detrimental to the sound

quality as it tends to stand out over broad band noises.

The pure tone produced by this oscillation suggests a resonance might be occurring [1]. The fluid-structure interactions of a poppet valve were modelled in [8] where the authors found that the axial vibrations were related to jet impingement length and poppet geometry.

Another instability comes from hydraulic jet flip. For low fluid velocities, the fluid sticks close to the surrounding walls while travelling through restrictions. At higher velocities, the fluid tends to separate from the walls. If the velocity is medium, the fluid will flip flop between these two distinct flow shapes, causing a flow ripple. This phenomenon produces a 'squeal' noise and can be avoided by operating at different conditions [1, 9]. If left unattended, these instabilities are self-sustaining, and the ripple they create may excite other resonances in the system.

2.1.1.4 Flow Noise

The motion of fluid is described as laminar or turbulent, which are distinguished by calculating the Reynolds number. Laminar flow is characterized by smooth stream lines of fluid travelling parallel to one another. Turbulent flow is characterized by random motion of the fluid with a velocity component perpendicular to the bulk fluid velocity direction. Turbulent flow produces more noise than laminar flow. However,

turbulence is unavoidable in hydraulic piping systems and must be accounted for when designing quieter hydraulics.

Turbulent flow noise in pipes mainly occurs due to boundary layer separation, vortex shedding and hydraulic jet noise. Turbulent flow through an orifice produces broad-band noise. The amplitude depends on the volume flow rate and back pressure [10] as well as cross sectional area. Lighthill [11] derived an expression for turbulent flow represented by a distribution of quadrupoles in a medium at rest.

Flow through an orifice produces a free jet which is surrounded by eddies formed at the jet boundaries. The minimum pressure in the jet occurs at the vena contracta. At this region, if the pressure is sufficiently low, cavitation may also occur. Several studies were performed measuring the noise spectra of cavitating orifices [12]. [12] also found that, for a thin orifice (for thickness t and diameter D given by $t/D < 1$), a whistling frequency in acoustic signals occurred which was not present for thicker orifices ($t/D > 1$) and was also not present in super-cavitating conditions due to cavitation noise being produced far downstream.

Cairns et al. [10] used a modified IEC method [13] compared with experimental results and found orifice cavitation noise matched within 2.5 dB between experimental and predicted results. They show FBN on a surface plot as a function of flow rate and back pressure. Their results show an increase in FBN with decreasing back pressure and/or increasing volume flow rate.

The turbulent boundary layer (TBL) is an important concept in the study of turbulence induced flow noise. Sound radiated by the turbulent boundary layer differs from the free turbulence model of a distribution of quadrupoles, and owing to the presence of the boundary layer is treated as a distribution of dipoles. G.M. Corcos developed an early model for the TBL to describe surface pressure. This model is closed form and requires little computational effort. The Corcos model tends to over-estimate the spectrum for low wavenumber [14] [15]. Graham noted the Smol'yakov-Tkachenko model improved on low wavenumber results but required greater computational effort [14].

Caiazzo et al.[16] [17] have proposed a generalized Corcos model to improve on low wave number results while retaining computational simplicity. This model replaces the Lorentz function of the Corcos model with a two-dimensional Butterworth filter. Careful selection of the orders for the Butterworth filter reduce low-wavenumber levels to 20 dB below the Corcos model which better match Smol'yakov-Tkachenko model. Caiazzo et al. use this model to predict noise transmitted to an enclosed space by a flexible plate driven by a TBL. The author found that use of the generalized Corcos model produced a good description of the spectrum in the convective domain [16].

Much study has been done on TBL generated noise. Hu et al. [18] computationally showed that the TBL generated noise at low mach numbers was primarily caused by fluctuating boundary stresses. Croaker et al. [19] developed a numerical model

for estimating flow induced noise, calibrated using data collected by Hu et al., that replicated the acoustic power produced by a submerged slender body.

2.2 Reynolds Number

The Reynolds number is a dimensionless parameter used in fluid dynamics. It is an expression relating inertial forces to viscous forces in a fluid. For fluid flow in a pipe, a Reynolds number of 2300 or less indicates laminar flow. A Reynolds number of 3000 or greater indicates turbulent flow. Values in between are in the transition region. The Reynolds number can also be used to determine if the inviscid assumption of a fluid is valid, as a Reynolds number greater than 1 means viscous forces are much less significant than inertial forces. The Reynolds number has many forms, of which this work used the form in Equation 2.5.

$$Re = \frac{Qd}{\nu A} \tag{2.5}$$

Where Q is the volume flow rate, d the cross section diameter, ν the kinematic viscosity, and A the cross section area of the flow restriction.

2.3 Froude Number

The Froude number is a dimensionless parameter expressing the ratio of inertial forces to gravitational forces in a fluid. The Froude number is calculated by

$$Fr = \frac{v}{\sqrt{gd}} \tag{2.6}$$

where v is the mean fluid velocity, g the acceleration due to gravity, and d the restriction diameter. The mean fluid velocity was calculated using volume flow rate by $v = Q/A$.

Turbulent flow noise will be the main focus of the flow noise component in this work. All tests performed were for turbulent flow according to the Reynolds number calculated from measured flow rate and cross section area.

Chapter 3

Methods and Materials

The MTU hydraulic test bench was developed to simulate a reference hydraulic circuit [2]. The test bench was developed to study the energy transfer of FBN to SBN through hose clamps and the physics of the FSI between the hydraulic oil and the hose walls. The pump flow ripple was characterized using ISO 10767-1 [3]. The reference circuit and test bench specifications are listed in table 3.1. The test bench components are discussed in detail here. Modifications made to the test bench are also discussed. The original test circuit is shown in Figure 3.1.

Figure 3.1: 2.13 m Hose Hydraulic Test Circuit for Mount Energy Loss Tests

3.1 Valve Test Bench Development

The MTU hydraulic test bench consists of an electric motor coupled to a Bosch Rexroth 28cc variable axial piston pump. The pump has a cutoff operating pressure of 2320 psi and a rated speed of 2100 RPM. Achieving the maximum reference hydraulic circuit maximum speed required over-speeding the pump. A 100 HP electric motor was chosen. A ABS ACS550 drive unit controls the motor speed via a wired remote.

The test bench was modified to install a solenoid controlled pilot-operated spool valve. The end-of-line loading valve was replaced with the spool valve. The 2.13 m hose was replaced with a hydraulic circuit that flows through the valve and supplies the valve

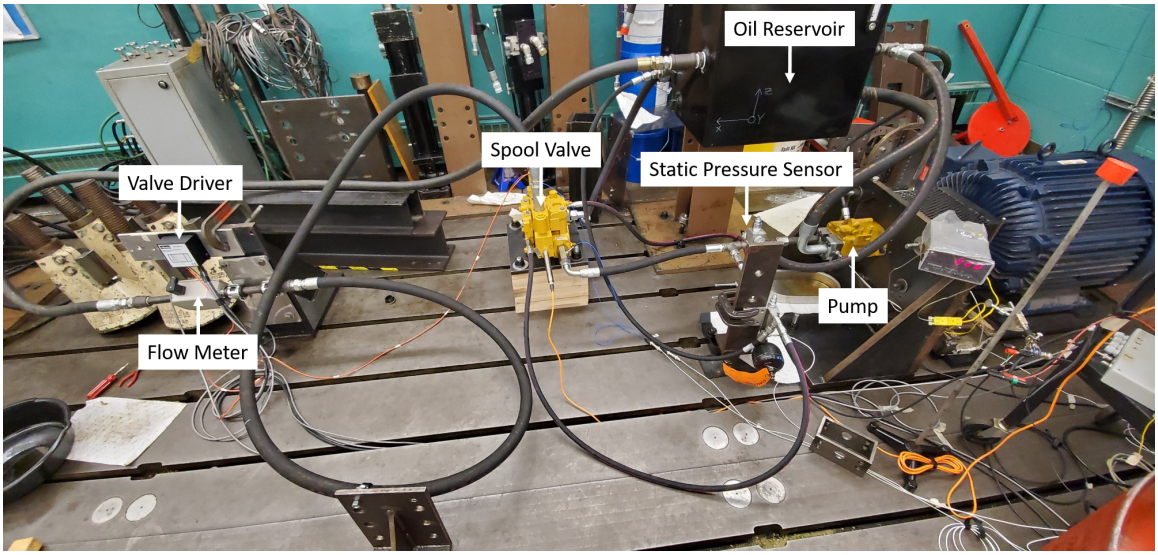

Figure 3.2: Modified Hydraulic Test Bench Circuit with Spool Valve

pilot. The new hydraulic circuit is shown in Figure 3.2. A complete parts list is found in Appendix A.

The MTU hydraulic test bench is capable of measuring the pressure ripple at the inlet and outlet ports of the valve under test. The SBN transferred to the valve mount currently is not being considered due to hardware limitations.

	Motor Speed [RPM]	Flow [GPM]	Power [HP]	Torque [Ft-Lb]
Reference Hydraulic Circuit	–	–	–	–
Test Bench Capabilities	0-2700	17.3	100	295 @ 1800 RPM

Table 3.1
Test Bench Requirements

Chevron Rando HDZ 32 hydraulic oil was selected because it was available at MTU. This oil closely matches the 10W oil used in the reference circuit, which is compared in table 3.2. A 25 gallon reservoir was mounted to a support next to the pump.

	Viscosity 40°C cSt	Viscosity 100°C cSt	Density g/cc	Bulk Modulus kpsi
HDZ 32 Reference	32 –	6.2 –	0.8433 –	285 –

Table 3.2
Hydraulic Oil Specifications

The oil temperature was monitored with a thermocouple attached to the end of the suction line.

3.2 Construction of Valve Circuit

Two sections of schedule 80 pipe (total length 14 inches) connected by a coupling are attached to the pump outlet port. The coupling is drilled and threaded to fit a dynamic pressure sensor. The pipe terminates at a housing for a direct acting pressure relief valve. The pressure relief valve returns to the reservoir through a section of SAE 100R6-12 hose. The first section of the circuit is shown in Figure 3.12.

A steel tee is connected to the through port of the pressure relief valve. One side of the tee connects a length of SAE -8 hosing to the pilot pressure reducing valve. The pilot pressure reducing valve provides pressure to the valve spool. Oil returning from the valve pilot returns to the reservoir through a section of SAE -6 hose. The other side of the tee connects to the valve inlet port with a 20 inch SAE -12 hose which terminates in a 90 degree steel elbow.

The valve inlet and outlet ports feature a 2 inch long adapter that was drilled and tapped to fit a dynamic pressure sensor. The adapters were chosen so that their inner diameter matched the hose and pump outlet port.

The valve was mounted with M12 bolts to a 3/4 inch steel plate. This plate was stacked on 3/4 inch medium density fiber boards so that the valve inlet port was level with the pump outlet port to minimize unneeded bends in the hose. Four threaded rods fasten the stack to the bedplates. Figure 3.11 shows the mount.

The end-of-line system consisted of a variable-area type flow meter and a length of SAE 100R3-16 hose returning to the reservoir. The spool valve test bench schematic is shown in Figure 3.3 with the primary components listed in Table 3.3

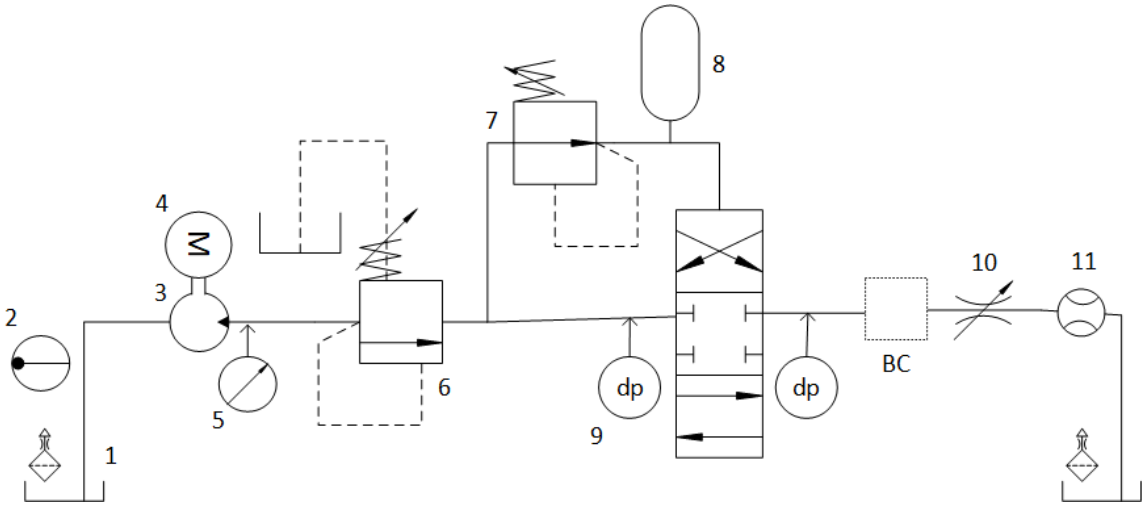

Figure 3.3: Spool Valve Test Bench Schematic

	Component	Description
1	Vented Oil Reservoir	25 Gallon
2	Thermocouple	Omega Type K
3	Axial Piston Pump	Bosch Rexroth LA10VO28 series
4	Electric Motor	100 HP - Marathon Y575
5	Static Pressure Sensor	Omega PX309-5KGV
6	Pressure Relief Valve	Sun Hydraulics RDFA-LAN
7	Pressure Reducing Valve	Sun Hydraulics PBDB-LBN
8	Accumulator	500 psi Charge
9	Dynamic Pressure Sensor	PCB Model 113B22
10	Needle Valve	Parker N1200S
11	Variable Area Flow Meter	Omega FLMH-3425SS-MA

Table 3.3
Spool Valve Test Bench Primary Component List

3.2.1 Construction of Orifice Circuit

Three orifices were tested having 3.50 mm, 5.02 mm, and 8.06 mm inner diameter. Each orifice was constructed by drilling the center from a 1/4" NPTF plug. This plug is fit inside an adapter with inner 1/4" NPTF threads. The adapter fit with the orifice is threaded for -8 STOR (F) to -16 STOR (M). The inlet line hose terminates in -12 ORFS female. Next in line is a -12 ORFS (M) to -12 ORFS (M) adapter is drilled and tapped to fit the inlet dynamic pressure sensor. Following is a -12 ORFS (F) to -12 ORFS (F) adapter. Following is a -12 ORFS (M) to -8 STOR (M) with inner threads to hold the orifice. Following is -8 STOR (F) to -16 STOR (M). Following is a -16 STOR (F) to -16 ORFS (M) which is drilled and tapped to fit the outlet dynamic pressure sensor. -8 To this last adapter the boundary condition hose under test is attached. All three boundary conditions begin with a length of -16 hose. The

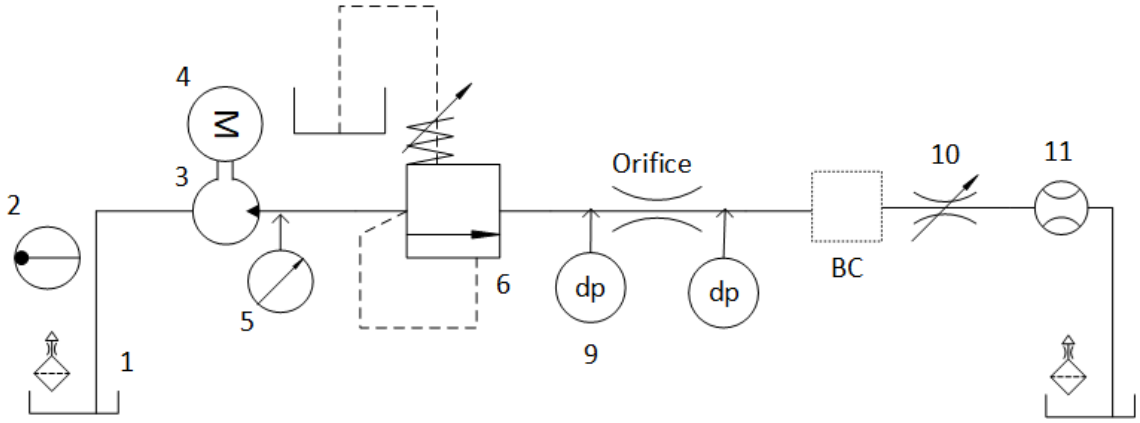

Figure 3.4: Orifice Test Bench Schematic

orifice setup is shown in Figure 3.8.

The needle valve boundary condition consisted of a 0.5 m length of SAE -16 hose connected from the valve outlet to a Parker N1200S needle valve. This needle valve was set to 4 intermediate positions from fully open to fully closed. For the fully open case, a secondary needle valve downstream of the flow meter was used to provide a 1000 psi system pressure needed for valve actuation (reference Figure 3.5). Tests were ran at 500 psi, 1000 psi, 1500 psi, and 2300 psi where the needle valve was fully closed.

The expansion chamber was constructed from a -24 steel pipe with -16 NPTF (F) and -12 NPTF (F) adapters welded to the ends. The total length of the chamber was 450 mm. The chamber was fitted to the valve with a 0.25 m length of -16 ORFS (F) to -16 NPTF (M) hose. The terminal end of the expansion chamber fit directly onto the flow meter inlet pipe. The expansion chamber is shown fixed to the orifice

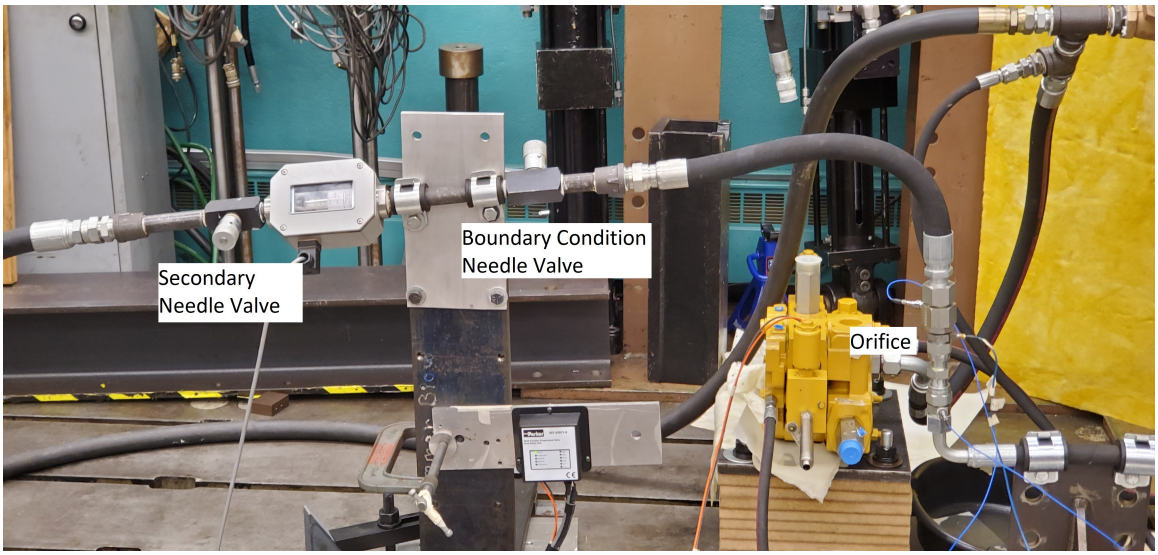

Figure 3.5: Closeup view of needle valve boundary condition being tested on orifice

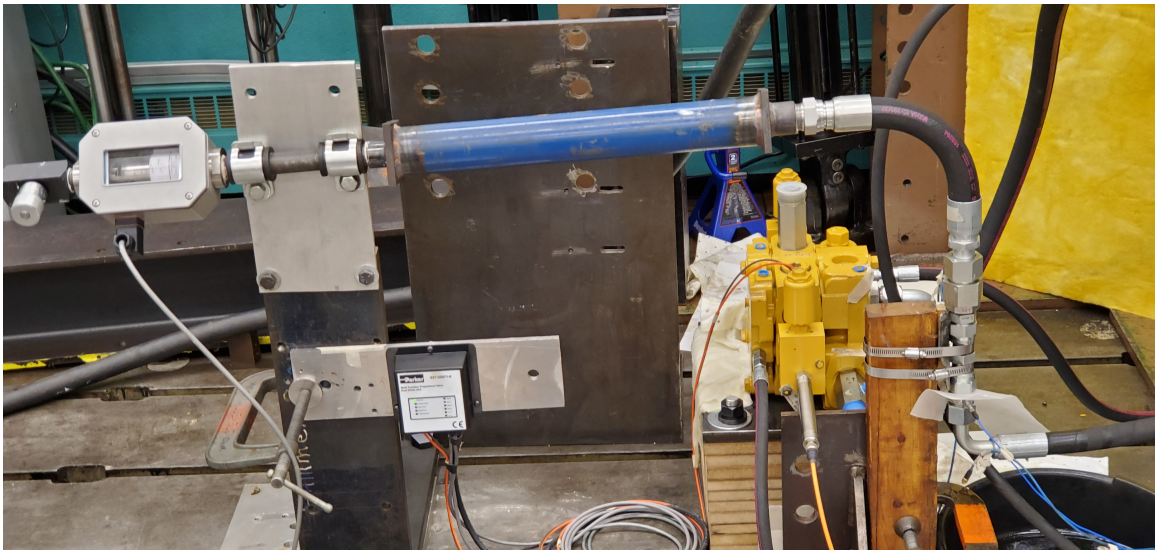

Figure 3.6: Closeup of Expansion Chamber Installed on Orifice.

in Figure 3.6.

The 4 meter hose boundary condition consisted of a 4 meter length of -16 hose starting with -16 STOR to -12 NPTF for fitting onto the flow meter inlet pipe with a female

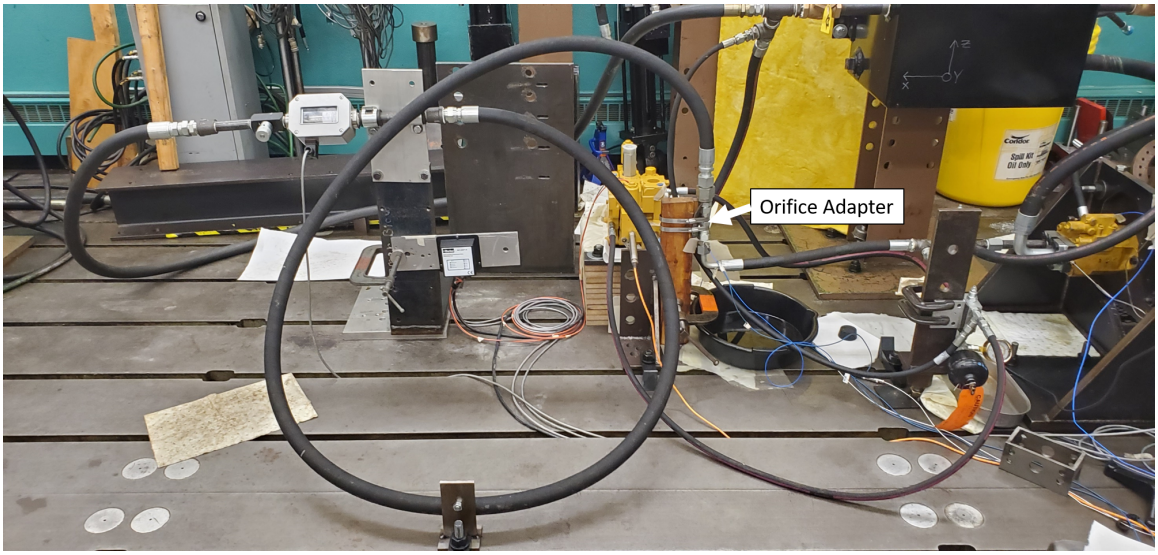

Figure 3.7: View of 4 Meter Hose Installed on Orifice.

to female -12 adapter. The 4 meter hose is shown fixed to the orifice in Figure 3.7.

The inlet line hose is mounted to the steel bedplates with P-clamps to ensure no travel occurs when the system is pressurized or experiences a change in static pressure. The terminal end of the test section at the flow meter is mounted with P-clamps. For longer boundary conditions (4 meter hose) it was necessary to include another mount at the midpoint of the length of hose for safe operation. Figure 3.5 shows the test setup for the needle valve boundary condition being tested on the orifice.

Figure 3.4 shows the test bench schematic. The primary components are listed in Table 3.3 in section 3.2 as the main components are nearly the same, with the exception of the removal of the pressure reducing circuit for the orifice tests.

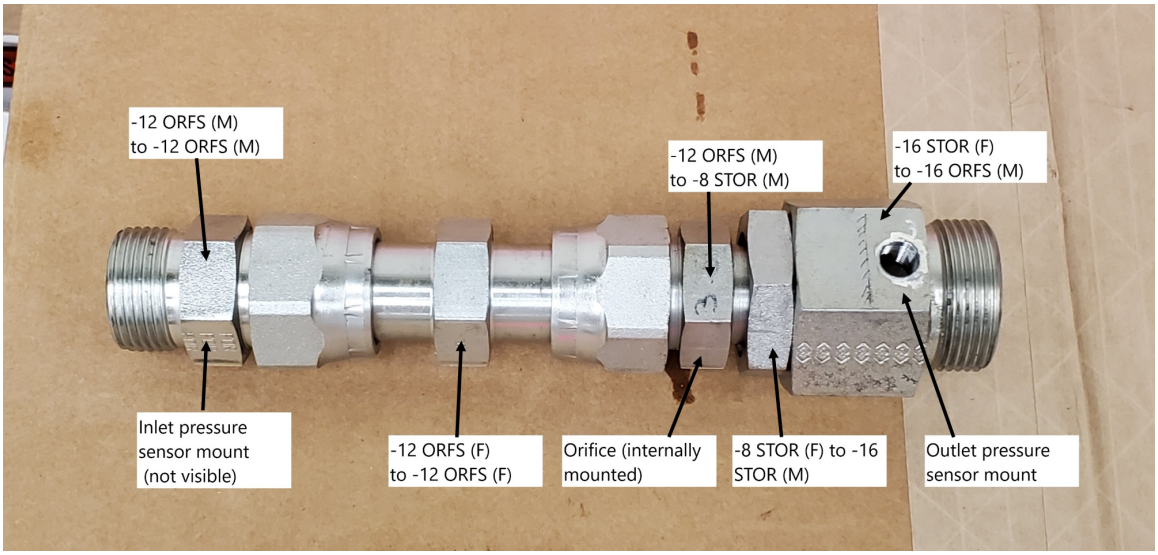

Figure 3.8: Orifice Housing and Pressure Sensor Locations on Adapters

3.3 Simple Orifice Assumption Comparison

It was desired to justify the assumption that the valve behaves like a simple orifice when producing flow induced noise. Pressure sensor data was collected on the valve and again with the valve replaced by an orifice having a fixed inner diameter. The valve flow noise was compared to the orifice flow noise.

Tests performed slowly swept the valve spool from fully closed to fully open under steady operating pressure and motor speed. See section 3.3.1 for a detailed test plan. The slow sweep rate minimizes transient events. The FBN as a function of spool position (which is related to the cross section of the valve port) was characterized.

The valve was swapped for an orifice and steady state data collected. These two data

sets were directly compared to see if the valve behaved the same as the orifice under the same operating conditions. Three orifices with different diameters were tested. The orifice diameters tested were 3.50 mm, 5.02 mm and 8.06 mm.

It was also desired to see the effects of post-valve boundary conditions on FBN. The BC may cause reflections of the pressure ripple and flow ripple. The boundary conditions tested are detailed in Table 3.4. Each boundary condition was tested on the valve and all three orifices. This resulted in 12 unique test configurations being tested.

3.3.1 Valve Area Sweep Test Procedure

Dynamic pressure sensor data was collected at the valve inlet and outlet ports. The system static pressure was measured at the pressure relief valve casing. The three motor speeds tested at were 1000 rpm, 1500 rpm, and 2000 rpm for all configurations. The expansion chamber and 4 meter hose boundary conditions were tested at 1000 psi and 2000 psi only. The needle valve boundary condition was tested at 4 intermediate settings from fully open to fully closed. These settings produced back pressure of 500 psi, 1000 psi, 1500 psi, and 2300 psi when fully closed.

Tests involved slowly sweeping the valve from fully closed to fully open. This minimized the likelihood of transient events occurring. This also minimized system

Component	Description	
4 Meter Hose Needle Valve Expansion-Contracti on Chamber	SAE -16 Parker N1200S Expansion Ratio 2.356	 Contraction Ratio 3.82

Table 3.4
Three Boundary Condition Specifications

changes during the 0.75 second measurement period. Run times were 60 seconds total. When the spool valve was fully opened, there was not enough of a restriction to provide the minimum static pressure needed to operate the valve spool. It was necessary to add an inline Parker N1200S needle valve. This secondary valve was set while the spool valve was fully open to ensure minimum static pressure was maintained.

3.4 Data Processing

All data sets were sampled at 20480 Hz with a 60 second total measurement time. Throughput data sets were exported from Testlab as a .mat file to be read by Matlab. The power spectrum was calculated. A window of 15360 samples were selected with a 50% overlap with the previous window. Figure 3.9 shows this schematically. A hanning window was applied when computing the power spectrum. It was necessary to filter some of the pressure sensor autopowers to remove electrical noise using a median filter due to bad grounding noise on DAC channels. See Appendix D for

a detailed discussion on electrical noise filtering. The LVDT signal measured in the valve sweep was converted from voltage to displacement then to area using a calibration factor and area curve.

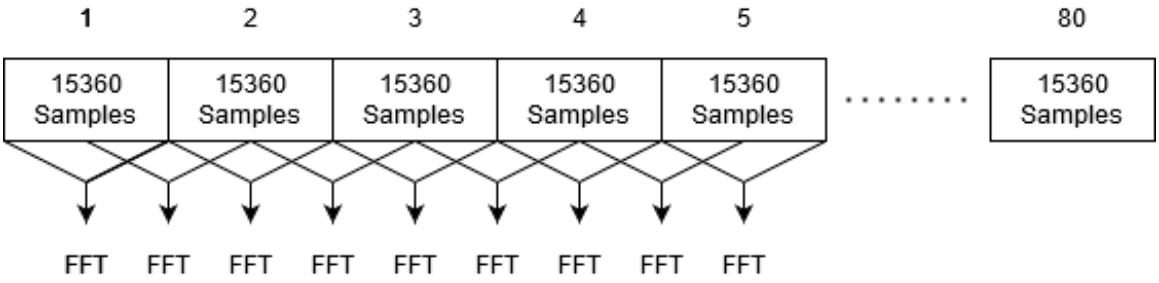

Figure 3.9: 50% Overlap Data Sampling Structure

The flow noise was calculated by summing each spectra of the outlet pressure sensors. The pump harmonics were filtered out using the measured motor speed which was converted to frequency. Pump harmonics were found using multiples of 9 of the rotational frequency. This produced the location of each harmonic, in Hz. Next, a bandwidth of N spectral lines around each harmonic was set, such that 2N spectral lines were three times wider than the main lobe. The harmonic peak was removed using a linear interpolation between the neighboring non-outlier data points.

With pump harmonics filtered out of each spectra filtered, and electrical noise filtered if needed, the entire spectra was summed. Summing produced a single value for the total pressure ripple at each sampling window. The orifice data points were averaged for each run, as no physical parameters are changing throughout a test. The valve data was not averaged as it was desired to see the total pressure ripple at each window,

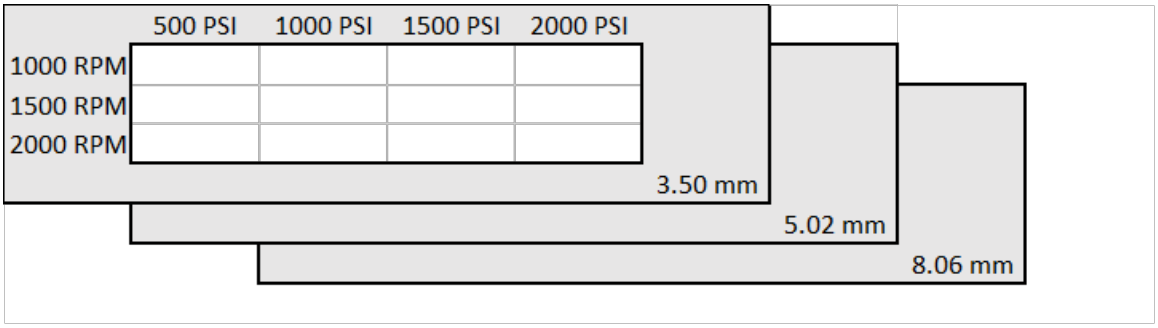

Figure 3.10: Visualization of Orifice Data Matrix Structure for a Single Boundary Condition

corresponding to a different cross section area.

Static pressure, cross section and flow signals were averaged over the same length of the window used to calculate the pressure sensor power spectrum with a 50% overlap of the previous window. This ensured the length of these signals matched the number of pressure data power spectra.

For directly comparing the valve and orifice at equivalent cross section areas, flow noise data from each boundary condition was stored in 3-dimensional matrix where the axes were (RPM,Pressure,Area) and the stored data was the flow noise amplitude. See Figure 3.10 for a visualization of this data structure. This allowed for quickly plotting two of the three dimensions to generate a surface, and visually compare the effect of volume flow rate, back pressure, and cross section area on flow noise.

3.4.1 Instrumentation

The primary measurement and control instruments are listed and described.

A RDP ACW model linear variable displacement transducer (LVDT) was connected to a RDP S7AC signal conditioner which provided a gain to the output voltage from the LVDT. The calibration factor was determined once the appropriate gain is selected. A gain was chosen such that a displacement of the LVDT rod of ± 10 mm produced a ± 5 volt signal. This gave a calibration of 0.5 V/mm of displacement.

The valve spool position was measured directly by threading the LVDT rod through the solenoid housing and onto the spool shown in Figure 3.11. Appropriate signal conditioning was applied to produce a voltage. This voltage is linearly related to the spool displacement and was converted to millimeter with the calibration factor. A manufacturer supplied spool displacement to surface area chart was used to calculate the effective valve opening surface area using Matlab. It was assumed that the diameter of the spool valve could be calculated by treating the cross section area as that of a circle and solving for the diameter.

PCB model 113B22 dynamic pressure sensors were used to measure the inlet and outlet dynamic pressure. They feature a nominal sensitivity of 1.0 mV/psi and have a pressure range up to 5 kpsi for ± 5 V output. Their operating temperature ranges

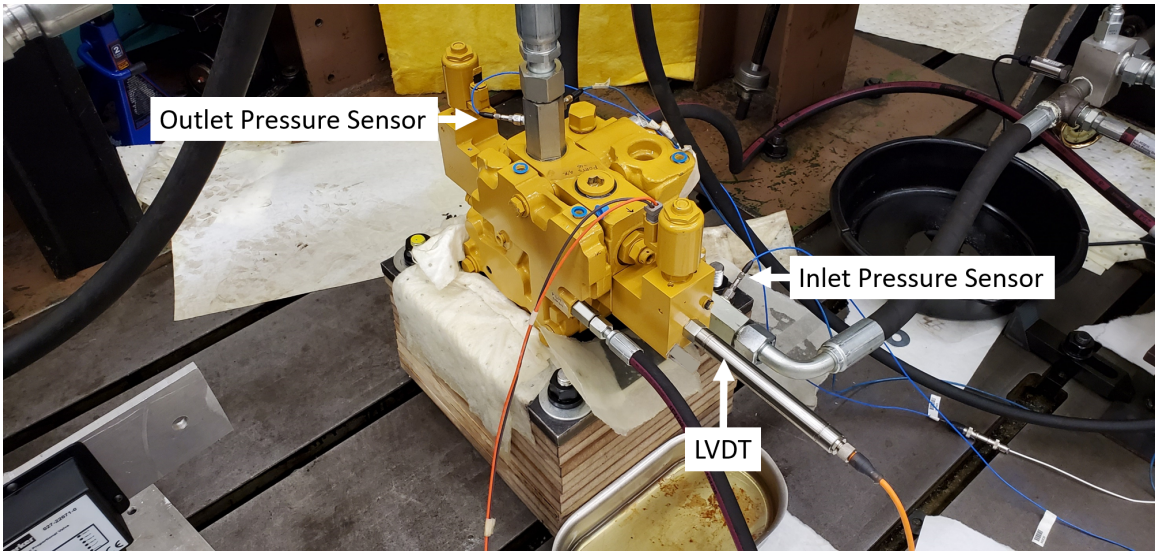

Figure 3.11: Transducer Locations on Spool Valve

from -73°C to +135°C, which is well above the maximum expected oil temperature of 60°C achieved at the end of a test.

The dynamic pressure was measured at the valve inlet and outlet. The pressure sensors were attached to a pipe coupling adapter that was drilled and threaded, reference Figure 3.11.

A Omega PX309-5KGV static pressure sensor was selected. This sensor has an operating pressure range of 0 to 5 kpsi gage and can withstand oil temperatures up to 85°C. The mean system pressure was measured at the pressure relief valve casing with a drilled and tapped hole as shown in Figure 3.12. The static pressure sensor serves as a monitor for the system operating conditions.

The speed of the motor attached to the pump was measured with a laser tachometer

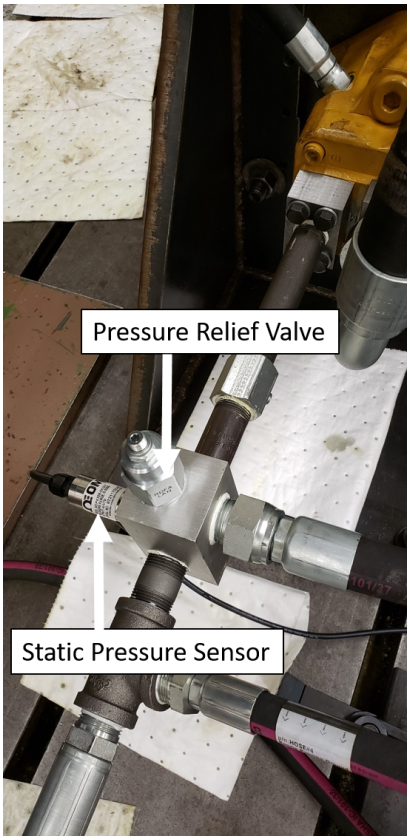

Figure 3.12: Static Pressure Sensor Location

directed at the shaft coupling. A 1 pulse/revolution marking was attached to the coupling. The tachometer was supplied a 2 mA current via an ICP signal conditioner. Reference Figure 3.13 for tachometer orientation.

The flow meter was a variable area type. It was used during testing as a control parameter for monitoring system operation and as a check for motor speed. Flow was also measured for analyzing how flow noise changed for different flow rates.

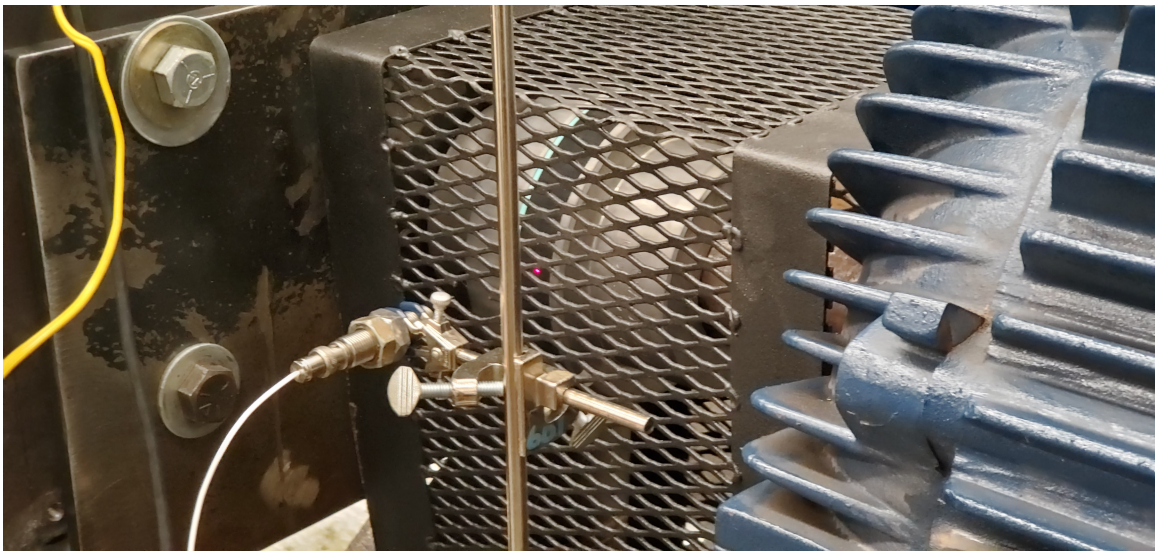

Figure 3.13: Tachometer Orientation on Motor Pump Coupling Showing Safety Cage

3.5 Test Bench Operation

System operating conditions were measured using a static pressure sensor, tachometer, and flow meter in LMS Testlab Signature Testing Advanced. The valve was controlled electronically by the operator with a potentiometer. Motor speed was set by the operator with a wired remote before testing. A complete wiring diagram is found in 3.14. The system pressure was set using a needle valve located after the flow meter.

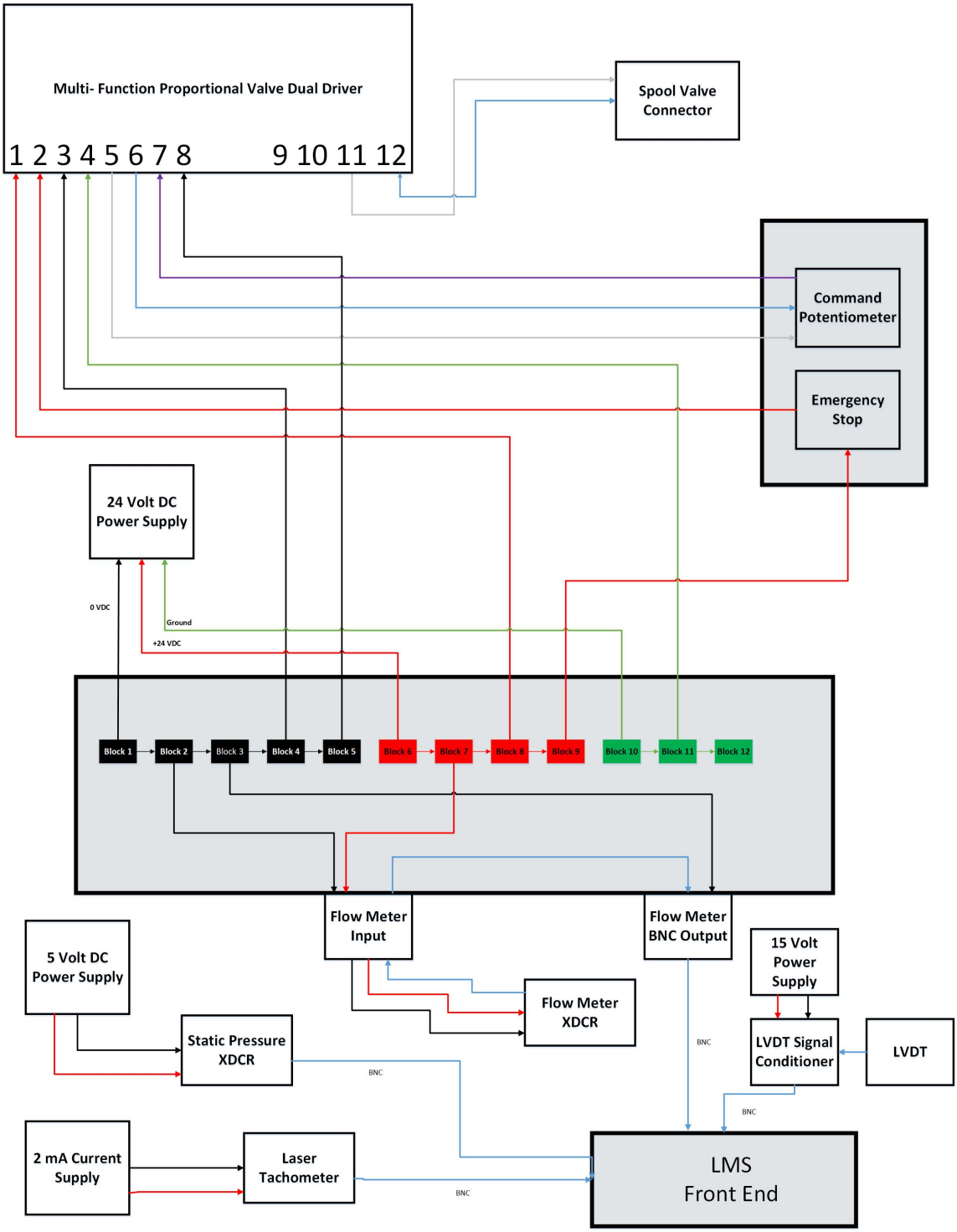

Figure 3.14: Valve Circuit Wiring Diagram

3.5.1 Test Bench Safety

The rotating component of the motor-pump coupling was enclosed in a metal cage to prevent loose items and cable from becoming entrapped. Separate kill switches for the valve and motor power supply were installed at the operator location in case of emergency. All hydraulic lines and components were selected to greatly exceed the maximum working pressure of 2300 psi set by the pressure relief valve. A spill relief kit was kept on hand.

3.6 Summary

The MTU hydraulic test bench was modified to fit a pilot operated spool valve. The post-valve boundary conditions could be easily swapped. Valve flow induced noise was measured with dynamic pressure sensors on each end of the valve. For the valve and all three orifices, three boundary conditions were tested.

Chapter 4

Results

Results of measuring dynamic pressure at the inlet and outlet for the valve and orifice set is discussed. Data processing methods are explained. Analysis focused on the outlet pressure sensor where turbulent flow noise generated by fluid travel through the restriction is present.

The valve and orifice data sets are compared for each boundary condition individually. The valve and orifice data is compared for equivalent cross section areas first to examine if the valve and orifice generate the same amplitude flow noise for equivalent cross section areas. The total flow noise generated by the valve under every test condition and boundary condition are plotted along with the results from the orifice. The valve flow noise is curve fitted and R^2 values are calculated to examine the

goodness of fit.

4.1 Needle Valve Flow Noise

The total flow noise can be viewed in a combined and overlaid plot to compare the valve with the orifices for any motor speed and static pressure. The x axis is the cross section area of the valve opening or the orifice, and is normalized by the inlet line hose cross section area. The y axis is the sum of the spectra and is normalized by the operating static pressure. Thus both x and y axes are dimensionless as shown in Figure 4.1.

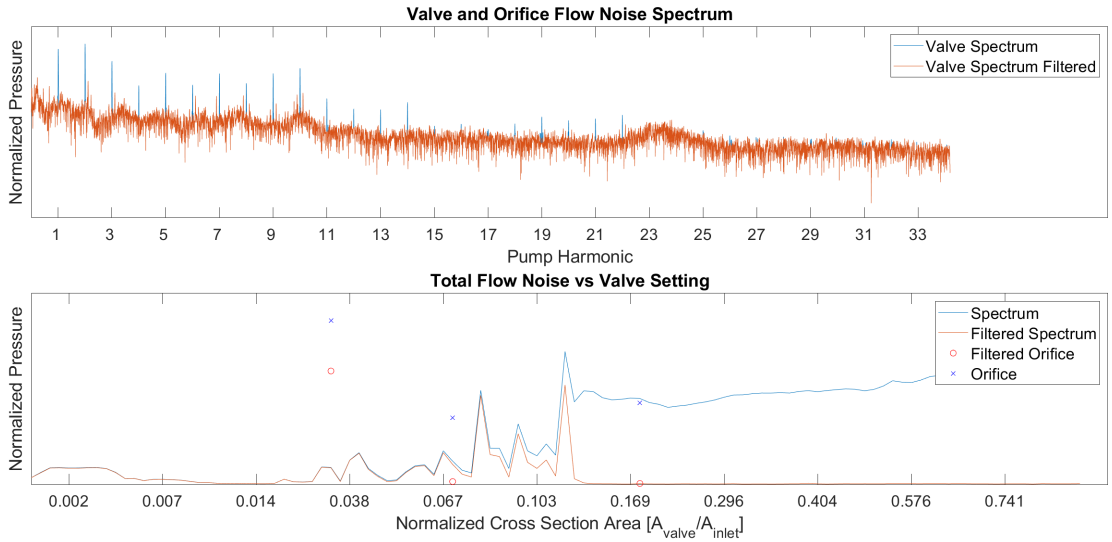

Figure 4.1: (Top) Needle Valve Boundary Condition - Valve Spectra With and Without Harmonics Filtered Out - 1000 PSI 2000 RPM.
(Bottom) Time series of normalized cross section area vs. normalized pressure comparing valve and orifices showing difference in amplitude for smallest orifice size.

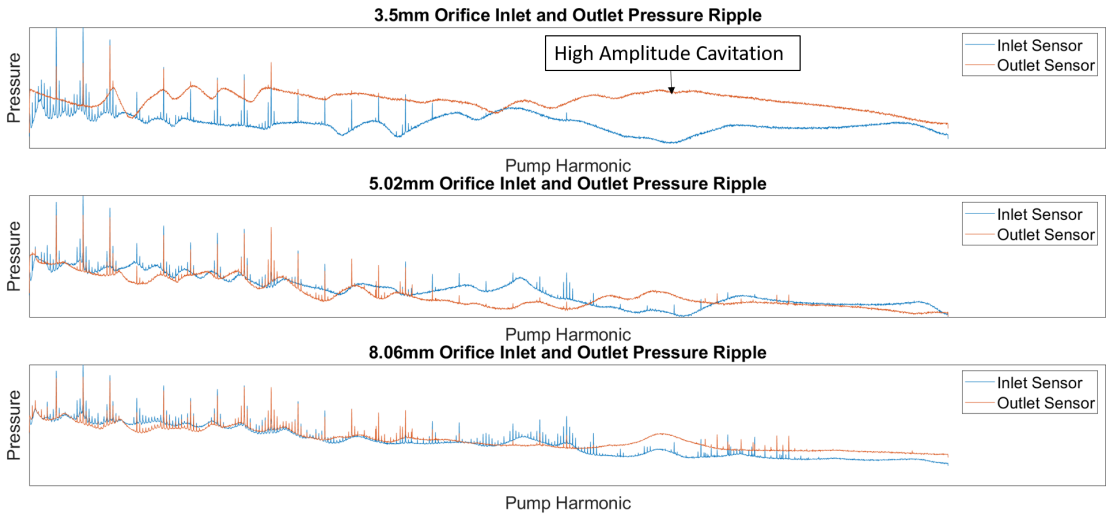

Figure 4.2: Spectra at Inlet and Outlet for 3.50 mm (Top) showing strong cavitation on outlet sensor, 5.02 mm (Mid) and 8.06 mm (Bottom) Do Not Produce Cavitation- 1000 PSI, 2000 RPM

The 1000 PSI and 2000 RPM set taken with the needle valve boundary condition is shown in Figure 4.1. Note that this figure shows both the filtered and unfiltered (pump harmonics removed) data and the x axis is evenly spaced in time. This operating condition shows the contribution of pump harmonics to the overall noise level. Pump harmonics are typically insignificant compared to the overall level for area ratios less than 0.05 to 0.1. The 5.02 mm and 8.06 mm orifices are both similar to the valve, while the 3.50 mm orifice differs greatly. This is the result of high volume flow rate through the small diameter orifice causing strong cavitation. The inlet and outlet pressure sensor spectra are plotted in Figure 4.2 where high amplitude broadband noise is seen in the outlet sensor vs. inlet sensor for the 3.50 mm orifice. Figure 4.3 shows the flow noise for 1500psi and 1000rpm where the orifice set and valve agree more closely. The spectra from the outlet dynamic pressure sensors are shown in

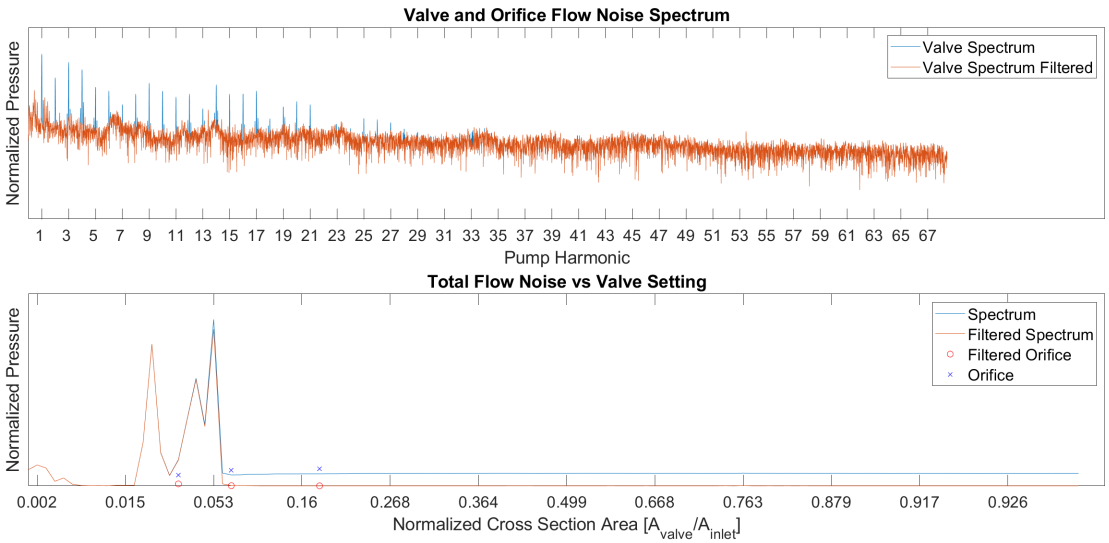

Figure 4.3: (Top) Needle Valve Boundary Condition - Dynamic Pressure Spectra at Valve Outlet - 1500psi - 1000rpm (Bottom) Agreement Between Smallest Orifice and Valve for Higher Back Pressure and Slower Motor Speed

Figure 4.4 for the 1500psi 1000 rpm test. The smallest orifice is not cavitating as severely as the 1000psi 2000rpm case, which leads to better match between the valve and orifice.

The total flow noise as a function of motor speed vs. cross section area or static pressure can be displayed as a surface. The cross section area and static pressure are selected to compare flow noise at 2000 rpm in Figure 4.5. This surface shows that the smallest orifice and valve differ significantly where the static pressure is low and volume flow rate is high. Also of note is that the flow noise increases with decreasing back pressure. This matches the results shown by Cairns [10]. The orifice data shows increasing flow noise with decreasing cross section area. For this range of cross sections, the valve does not show this same trend and instead peaks at the 2nd

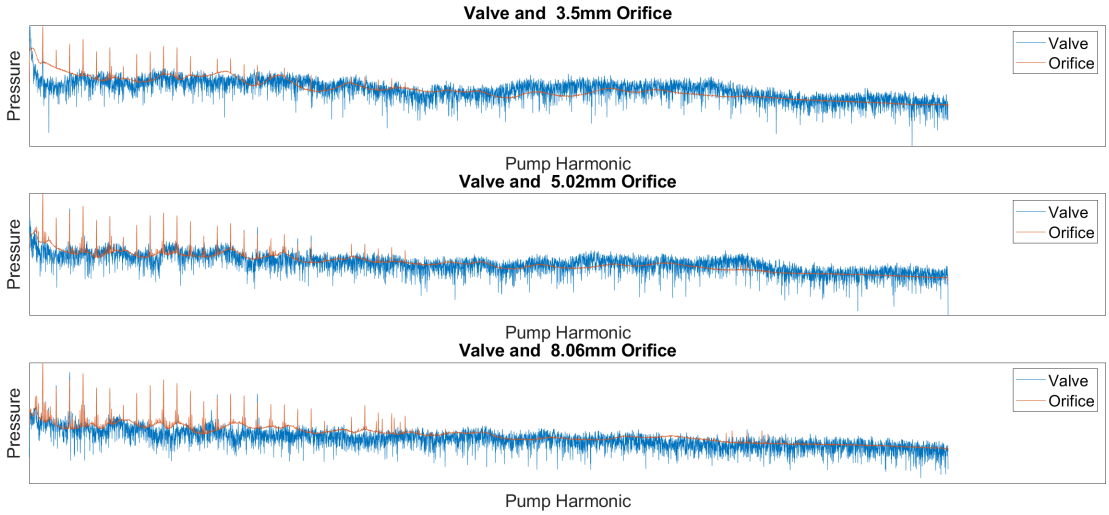

Figure 4.4: Spectra at Outlet for 3.50 mm (Top), 5.02 mm (Mid) and 8.06 mm (Bottom) Overlaid with Valve Showing Similar Autopower Spectrum - 1500 PSI, 1000 RPM

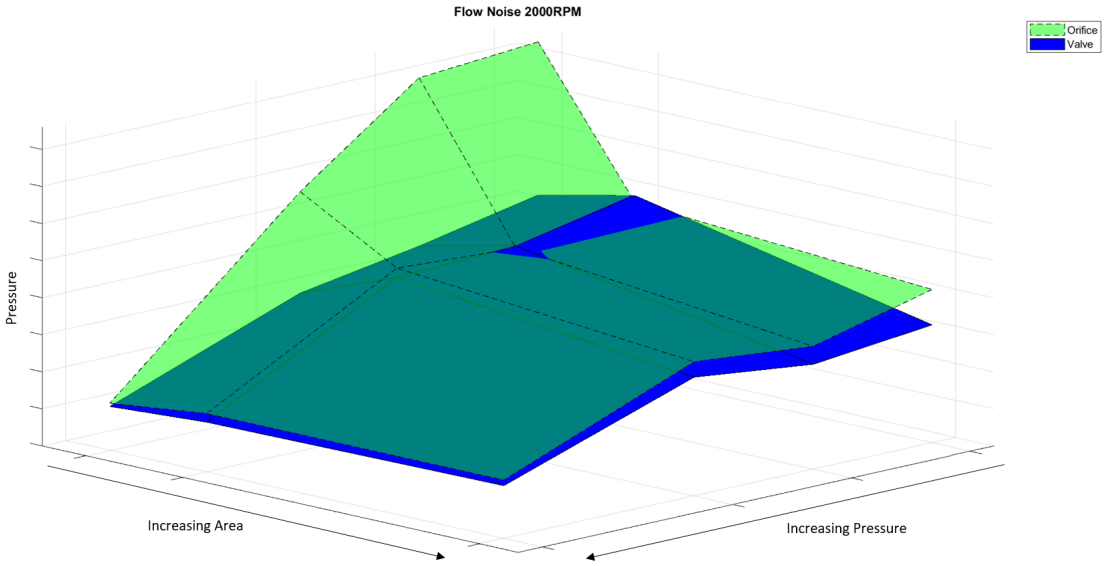

Figure 4.5: Flow Noise as a Function of Cross Section Area and Static Pressure for 2000 RPM Test - Needle Valve Boundary Condition.

cross section area.

4.2 Expansion Chamber Flow Noise Results

The flow noise vs. cross section area for the expansion chamber is plotted in Figure 4.6 for the 1000psi and 1000 rpm case. Here the flow noise follows a similar trend to that of the needle valve boundary condition in this test case. The expansion chamber had the most noticeable effect on flow noise when examining the spool valve. In several test cases, the flow noise showed a second peak between area ratios of 0.05 to 0.1 of higher amplitude than the orifices. This was unexpected based on the results from the needle valve boundary condition tests.

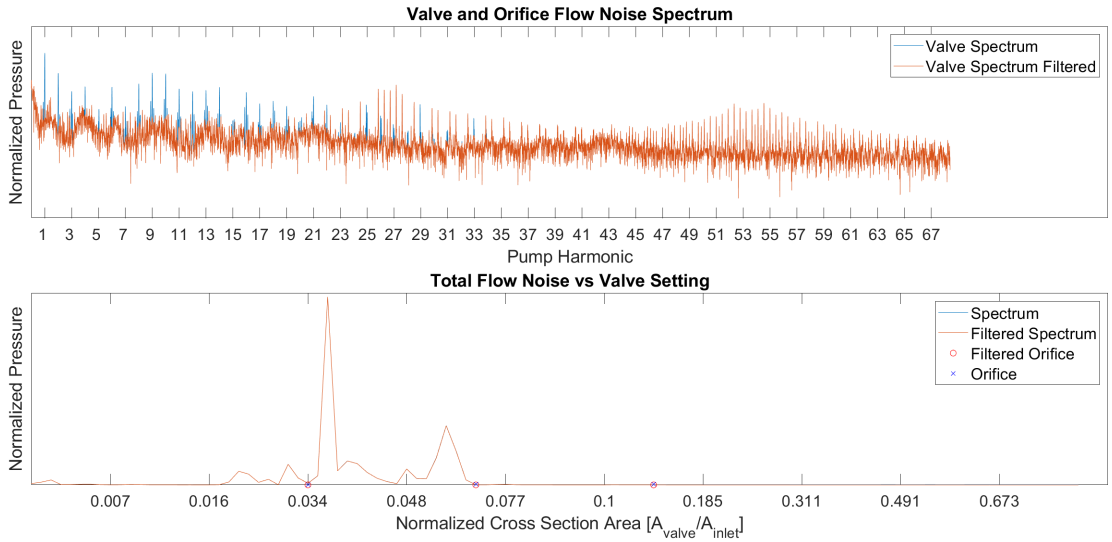

Figure 4.6: Flow Noise vs. Cross Section Area - 1000 psi 1000 rpm - Expansion Chamber

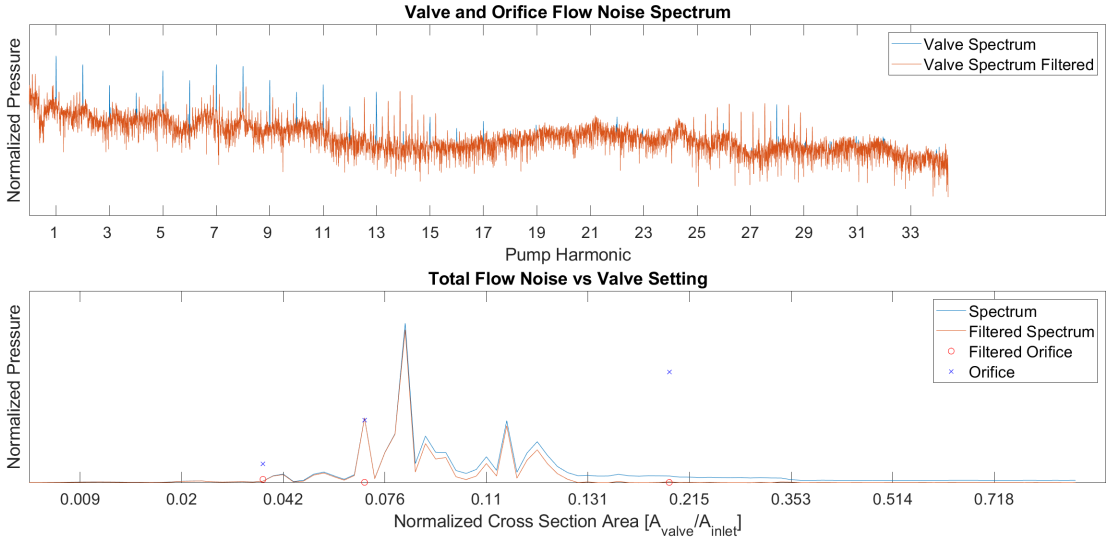

Figure 4.7: Divergence in Valve and Orifice Flow Noise - 2000 psi 2000 rpm - Expansion Chamber

It is still not clear why the expansion chamber produced high amplitude flow noise over a broader range of area ratios than the other boundary conditions. Figure 4.7 shows the 2000 psi 2000 rpm case where the flow noise peaks near 0.1 and does not match closely with the 3.50 mm or 5.02 mm orifice. The results converge for higher area ratios and the valve and 8.06 mm orifice match.

4.3 4 Meter Hose Flow Noise Results

The 4 meter hose boundary condition was not observed to change the flow noise response of the valve in comparison to the needle valve boundary condition. All tests performed displayed the expected area vs. flow noise response seen on the needle valve, shown in Figure 4.8 for the 2000 psi and 2000 rpm test. This test produced a

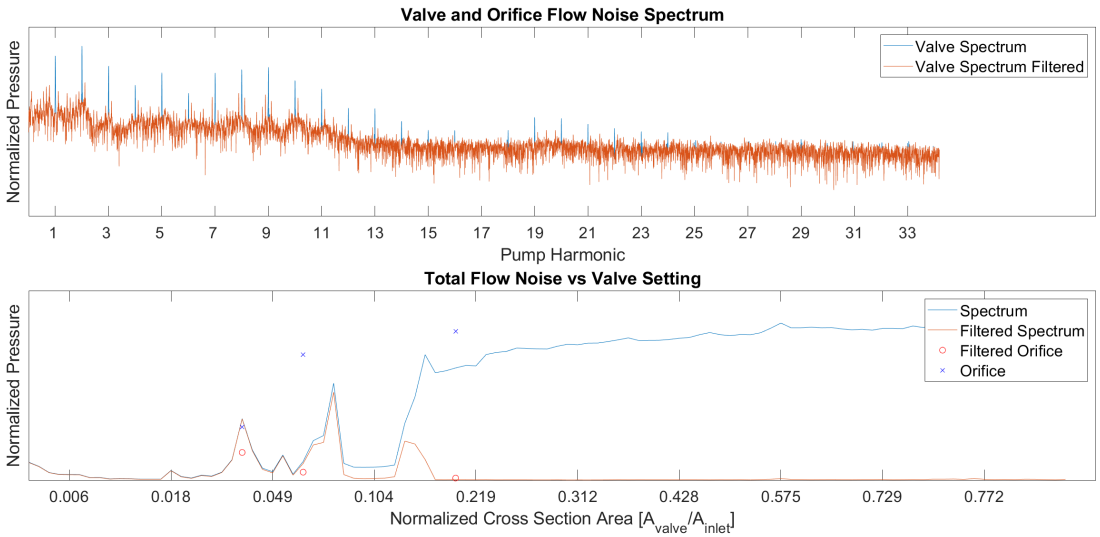

Figure 4.8: Flow Noise vs. Cross Section Area with Difference in Small Orifice Amplitude Due to Cavitation - 2000 psi 2000 rpm - 4 Meter Hose

different response when performed on the expansion chamber.

4.4 Flow Noise Dependence on Static Variables

The flow noise generated by the valve is compared with the instantaneous volume flow rate and static pressure. It was observed that the volume flow rate and static pressure both changed significantly while the valve spool was displaced. The static pressure tended to drop rapidly as the volume flow rate reached its maximum value. The volume flow rate increased quickly until settling at a steady value for the remainder of the area sweep.

Figure 4.9 compares the static pressure and volume flow rate change over the span

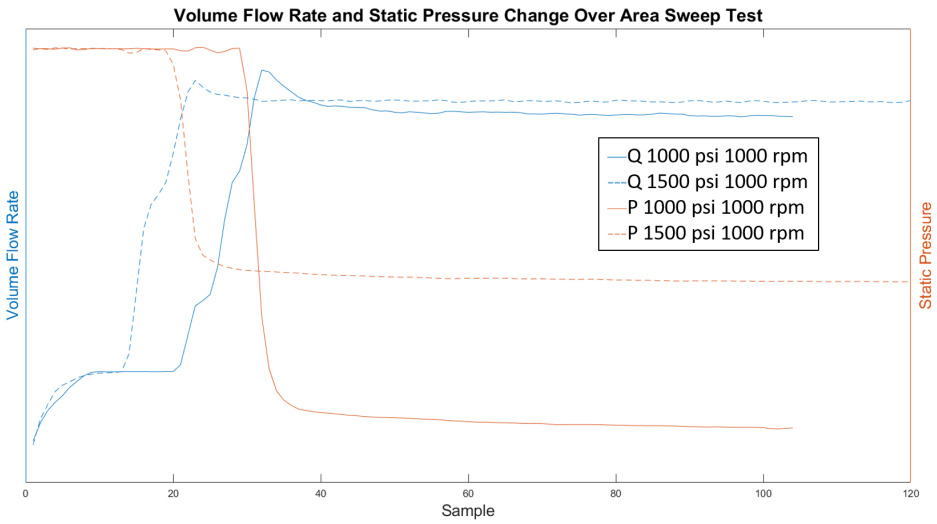

Figure 4.9: Evolution of Volume Flow Rate and Static Pressure for 1000 psi and 1500 psi - 1000 RPM Tested on Needle Valve.

of two tests both at 1000 RPM and 1000psi and 1500 psi. Sample 0 was taken from when the valve spool just cracked open and positive volume flow rate was observed.

In this region of spool travel where the flow rate and static pressure are changing, the total flow noise shows high amplitude. The 1000 psi and 1500 psi tested at 1000 RPM cases are compared in Figure 4.10. The region of high amplitude flow noise is referred to as the valve behavior transition region. The clustering of points in Figure 4.10 shows that the flow noise amplitude becomes steady when the volume flow rate and static pressure reach a steady value.

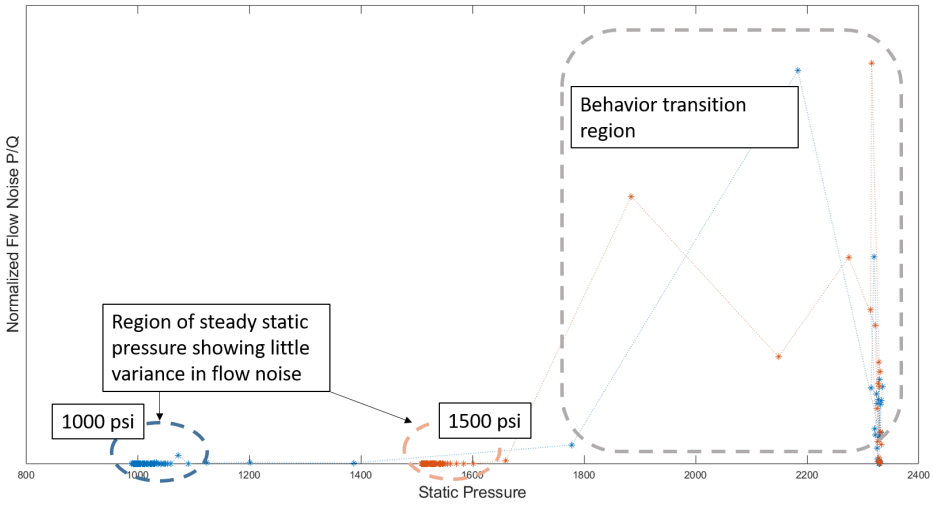

Figure 4.10: Normalized Flow Noise Amplitude vs. Static Pressure for 1000 psi and 1500 psi at 1000 RPM Tested on Needle Valve.

4.5 Combined Results

The full set of flow noise measurements for all volume flow rates, static pressures, cross section areas and boundary conditions are plotted in Figure 4.11 against the Froude number. The valve and orifice data are overlaid for comparison. We see strong grouping based on volume flow rate, which corresponds to motor speed. There is some variation within the volume flow rate clusters due to static pressure. The 500 psi case from the needle valve tests tended to produce higher amplitude flow noise when compared with the 1000 psi and 1500 psi tests for same volume flow rate, which was observed in previous results.

Normalizing the data by dividing by volume flow rate collapsed these results so that

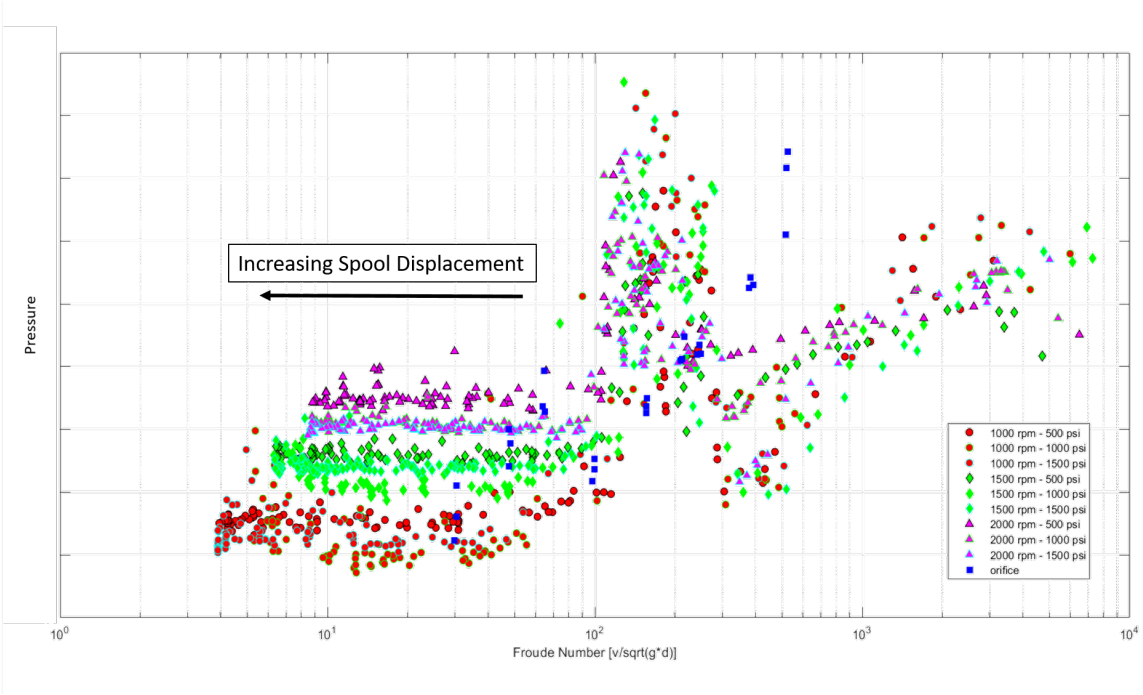

Figure 4.11: Full Flow Noise Data Set Showing Distinct Clusters Based on Volume Flow Rate

there were no longer distinct clusters. This is shown in Figure 4.12. Normalizing by volume flow rate also collapsed the orifice data onto the valve in the Froude number region above 300.

A distinct region of high amplitude flow noise that occurred between Froude numbers of 100 and 300 on the valve data set was identified. This region occurred over a narrow range of Froude number and does not show any identifiable trends. This region, referred to as valve behavior transition region, was not present in the orifice data sets. This suggests it was a characteristic of the valve spool travel, or some dynamic of the valve that is not present on the orifices that produced this noise in the valve. This region corresponded to the initial opening stages of the valve. A rapid

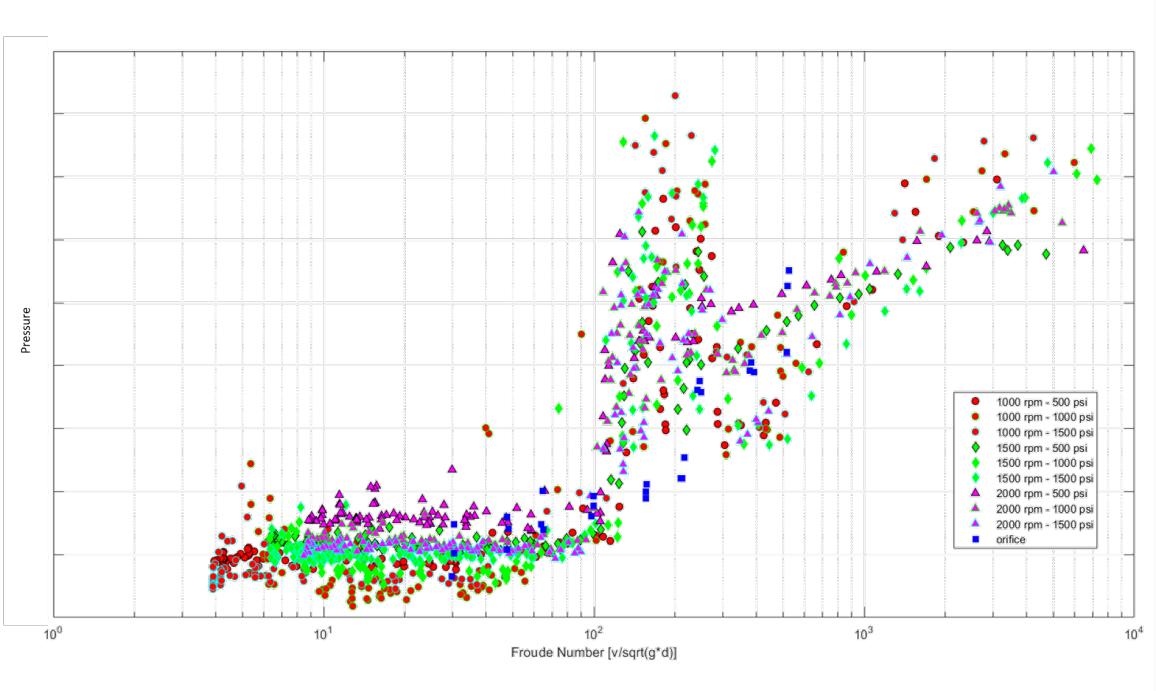

Figure 4.12: Full Flow Noise Data Set Normalized by Volume Flow Rate

change in the static pressure and the volume flow rate accompanied this behavior, as shown in Figure 4.9 and Figure 4.10. This region was excluded from curve fitting, and the two regions separated by the transition region were fitted separately.

The data was fit in two separate regions. For Froude number ≤ 100 a linear fit of the form $ax + b$ was used. For Froude number ≥ 300 a power fit of the form $ax^b + c$ was used. These fits are plotted over the data in Figure 4.13. The coefficient values and corresponding R^2 values are listed in Table 4.1.

The linear fit matched well with the orifice data in both regions. The fit in the high Froude number region showed an R^2 value of 0.6805 and matched well with the data trend for both the valve and orifices. The lower Froude number region showed an R^2

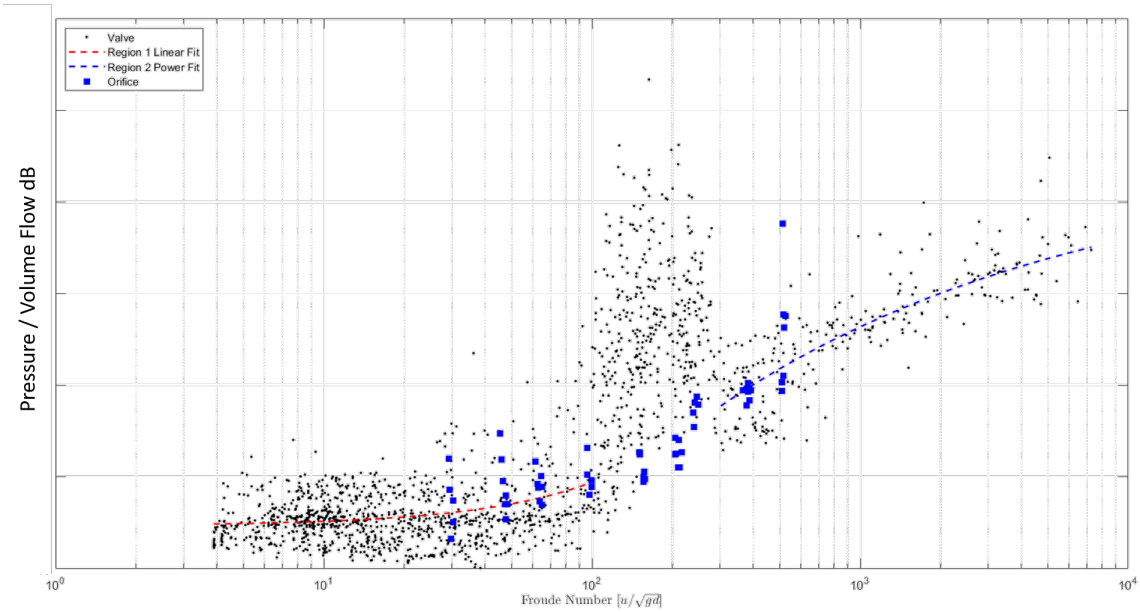

Figure 4.13: Froude Number vs Normalized Flow Noise with Region Curve Fits for All Boundary Conditions.

	Fit Coefficients	R^2 Value
Fr $\leq$ 100	$0.047x + 14.70$	0.0973
Fr $\geq$ 300	$-168.61x^{-0.32} + 54.85$	0.6805

Table 4.1
Coefficients from Curve Fitting and Corresponding R^2 Values

value of about 0.1. High variance in the flow noise amplitude within this region lead to a poor R^2 value.

4.6 Summary

The total flow noise produced by the valve and orifice matched closely for equivalent cross sections in most cases. However, there were cases where significant deviation

occurred, particularly for the smallest orifice size. This tended to occur at larger volume flow rates and lower back pressures, which matched results seen in literature.

When plotting the Froude number vs total flow noise for all conditions, clustering was observed that distinguished tests with different volume flow rates. Normalizing total flow noise by volume flow rate collapsed these plots and it was possible to develop a single empirical equation for low and high Froude number regions that was independent of boundary condition. A piecewise fit was chosen, as the valve data exhibited a behavioral transition region between $100 \leq Fr \leq 300$. This region was characterized by high and random amplitude, making curve fitting not possible. The linear function fit on the low Froude number region matched well with the observed trend, but had poor R^2 value of less than 0.1. This region still showed significant variance even within groups of similar volume flow rate. The high Froude number region was fit with a power function. This fit matched the data trend well and had an acceptable R^2 value near 0.7.

Chapter 5

Conclusions

This project adapted the MTU hydraulic test bench to test the flow noise characteristics of a spool valve and set of orifices. A variety of test configurations were implemented to examine the contributions of volume flow rate, static pressure and cross section area. These tests were repeated on three post-restriction boundary conditions and found little contribution from the boundary conditions.

First analysis comparing cross section with flow noise showed pump harmonics were not a dominant contributor to flow noise for area ratios below 0.05 to 0.1. Above this, filtering out pump harmonics noticeably lowers the total flow noise at the down stream dynamic pressure sensor. Pump harmonics were removed to assess only flow induced noise.

Back pressure had some effect on total flow noise. On the needle valve boundary condition, flow noise observed with 500 psi back pressure had slightly higher amplitude than the 1000 psi or 1500 psi cases. There was no observable difference in flow noise amplitude between the 1000 psi and 1500 psi cases. The results did show an increase in total flow noise with increasing volume flow rate, matching the results of Cairns [10]. Lower back pressure also tended to distinguish the valve from the 3.50 mm orifice due to cavitation from the orifice which was not observed on the valve. Dynamic pressure signals normalized by volume flow rate collapsed the data across different volume flow rates.

The collapsed data showed good agreement between the valve and orifice flow noise outside of the valve behavior transition region. Curve fitting these normalized flow noise points produced an empirical set of functions to estimate the flow noise. The steady state region at low Froude number showed variation. The higher Froude number region was fit with a power function and R^2 of 0.6805 was observed. It was necessary to apply a piecewise fit to the valve data as there was a transition region characterized by high amplitude flow noise occurring at the middle range of the Froude number scale tested.

This research showed that the orifice flow noise converged with the valve flow noise outside of the valves behavior transition region. Therefore the orifice model should provide a good estimate for the valve flow noise in the hydraulic circuit design stage.

The orifice did not exhibit the behavior transition region on the valve occurring at mid range Froude number. There is likely a stick-slip phenomenon or some other non-linearity occurring within the valve spool housing at these corresponding displacements. This was suggested by the static pressure measurements which showed transient peak events near locations in spool travel where high amplitude flow noise was observed.

Future work should seek to improve the empirical models by normalizing for different static pressures. The different boundary conditions showed little impact on the flow noise amplitude. Normalizing the flow noise magnitude by Q^n, for some undetermined value n, may also reduce the variance. Some aeroacoustic flow noise models include a Q^4 or Q^6 term which could be attempted with this data.

The dynamics of the valve should be explored further and characterized experimentally. Understanding the mode shapes and natural frequencies of the valve would lead to a better understanding of the contributions of SBN to flow noise. This could reduce variance in the low Froude number region. As turbulent noise is stochastic, it was expected that each individual spectra from the valve, which were not averaged, may not be locally accurate, but that taking the sum of the spectra would reduce these inaccuracies. However, the orifice data sets, which were averaged, showed similar variance.

Performing flow noise measurements on the valve for static cross section areas could

improve flow noise amplitude accuracy. Performing the tests at a static cross section will eliminate the effects of area smearing apparent in area sweep tests. Many simultaneous measurements could be performed, and the spectra averaged. Selecting a set of static cross section areas to test on the valve could also improve flow noise measurements by reducing dynamics associated with spool travel. The effect of system back pressure could be explored further. Currently, a difference in flow noise resulting from back pressure is only seen on the 500 psi case measured on the needle valve where the flow noise trended higher than in the 1000 psi and 1500 psi cases. A set of tests performed at smaller static pressure intervals which static pressure corresponded with the onset of steady flow noise. For a steady cross section area and motor speed, the static pressure could also be slowly swept via the needle valve installed after the spool valve to watch for a change in flow noise amplitude.

Test methods and metrics developed in this work can be used to examine the effects of active and passive FBN noise reduction mechanisms. The knowledge gained through this research will help in the design stage for future hydraulic systems.

References

[1] Stan Skaistis. *Noise Control of Hydraulic Machinery.* M. Dekker, 1988.

[2] Benjamin Kolb. Experimental characterization of hydraulic system sound. Master's thesis, Michigan Technological University, Dept. of Mechanical Engineering - Engineering Mechanics, 2019.

[3] Hydraulic fluid power — Determination of pressure ripple levels generated in systems and components — Part 1: Method for determining source flow ripple and source impedance of pumps. Standard, International Organization for Standardization, October 2015.

[4] K A Edge and T J Wing. The measurement of the fluid borne pressure ripple characteristic of hydraulic components. *Proceedings of the Institution of Mechanical Engineers, Part B: Management and engineering manufacture*, 197 Issue 4:247–254, 1983.

[5] B. K. Sreedhar, S. K. Albert, and A. B. Pandit. Cavitation damage: Theory and measurements – a review. *Wear*, 372–373:177–196, 2 2017.

[6] Y. Yan, R.B. Thorpe, and A.B. Pandit. Flow regime transitions due to cavitation in the flow through an orifice. *International Journal of Multiphase Flow*, 16:1023–1045, 1990.

[7] PracticalEngineering. *What is Water Hammer?* YouTube, https://www.youtube.com/watch?v=xoLmVFAFjn4, Nov 28, 2017.

[8] Wei Min, Hong Ji, and Linfeng Yang. Axial vibration in a poppet valve based on fluid-structure interaction. *Journal of Mechanical Engineering and Science*, 229(17):3266–3273, 2015.

[9] J. Blackburn, J Coakley, and F Ezekiel. *"Transient forces and valve instability" in Fluid Power Control*. The Technology Press of M.I.T., 1960.

[10] C. Cairns, R. J. Whitson, P. Strachan, and M. Wheel. Prediction of noise generated by orifice plates in liquid systems using a modified form of iec 534-8-4:1994. *Advances in Fluid Mechanics III*, 29:675–686, 2000.

[11] Michael Lighthill. On sound generated aerodynamically ii. turbulence as a source of sound. *Proceedings of the Royal Society of London*, 222:1–32, 1954.

[12] P. Testud, P. Moussou, A. Hirschberg, and Y. Auregan. Noise generated by

cavitating single-hole and multi-hole orifices in a water pipe. *Journal of Fluids and Structures*, 23:163–189, 2007.

[13] Industrial-Process Control Valves - Part 8: Noise Considerations - Section 4: Prediction. Standard, International Electrotechnical Commission, Geneva, CH, 1994.

[14] William R. Graham. A Comparison of Models for the Wavenumber-Frequency Spectrum of Turbulent Boundary Layer Pressures. *Journal of Sound and Vibration*, Vol 206 Issue 4:541–565, 1997.

[15] Teresa S. Miller. *Turbulent boundary layer models for acoustic analysis.* PhD thesis, Wichita State University, College of Engineering, Dept. of Aerospace Engineering, 2011.

[16] Anna Caiazzo, R D'Amico, and W Desmet. Use of a Generalized Corcos Model to Predict Flow-Induced Noise in a Cavity-Plate System. *International Conference on Noise and Vibration Engineering*, 2016.

[17] Anna Caiazzo, R D'Amico, and W Desmet. A Generalized Corcos Model for Modelling Turbulent Boundary Layer Wall Pressure Fluctuations. *Journal of Sound and Vibration*, 372:192–210, 2016.

[18] Zhiwei Hu, Christopher L Morfey, and Neil D Sandham. Sound radiation from a turbulent boundary layer. *Physics of fluids (1994)*, 18(9), 2006.

[19] P. Croaker, A. Skvortsov, and N. Kessissoglou. A simple approach to estimate flow-induced noise from steady state cfd data. *Proceedings of Acoustics*, pages 1–8, 2011.

[20] Gerhard Reethof. Turbulence generated noise in pipe flow. *Annual Review of Fluid Mechanics*, 10:333–367, 1978.

Appendix A

Test Configuration Component List

A.1 Spool Valve

Full components for the hydraulic spool valve test configuration are listed.

Component	Part Number	Description	Manufacturer
Power Unit			
Motor	ACS550	Drive Unit	ABB
Electric Motor	405THFS8036	100 HP 3-Phase	Marathon Motors
Motor Side Coupling	M70022824	2 7/8 - 3/4 keyed shaft	Magnaloy
Elastomeric Spider	M770H5	–	Magnaloy
Pump Side Coupling	M700A1316	13T splined shaft	Magnaloy
Hydraulic Circuit			
Reservoir	–	25 Gallon	Buyers
Globe Valve	–	Reservoir Shutoff	Milwaukee Valve
Reducer	–	1 1/4 - 2 NPTF reducer	
Tee Adapter	–	1" x 3.4" x 3/4"	
Suction Hose	–	SAE 100R6-20	
Gauge Port Block	Main 2303-20-20	-20 C61 gauge port block	Main Mfg.
Pump	LA10VO28DR/52L-VSC-11N00-S1608	28cc Axial Piston Pump	Bosch Rexroth
Case Drain Hose	–	716 -8 to -8 STOR	
NPTF Block	Main 1149-12-12M10	3/4 NPTF Block	Main Mfg.
Sch. 80 Pipe	–	6 inch	
Pipe Coupling	GG	3/4 GG NPTF	Parker
Sch. 80 Pipe	–	3 inch	
Cartridge Manifold	CLD	Through port with gauge port	Sun Hydraulics
Direct-Operated Relief Valve	RDFA-LAN	Direct operated relief valve	Sun Hydraulics
Sch. 40 NPTF T	–	Sch. 40 NPTF T	
Adapter	–	-12 NPTF to -10 STOR	
Pressure Relief Hose	–	SAE 100R6-12	
Pipe Nipple	–	3/4 to 3/4 NPTF	
Pressure Reducing Hose	–	SAE 100R6-8	
Cartidge Manifold	EAK	Through port with gauge port	Sun Hydraulics
Direct Operated Pressure Reducing Valve	PBDB-LBN	Pressure Reducing Valve	Sun Hydraulics
Adapter	–	-10 ORFS -10 STOR	
T Adapter	–	-10 ORFS(M,F) -8 STOR (P)	
Accumulator	–	-8 STOR	
Pilot Supply Hose	–	SAE 100R6-10	
Pilot Adapter	–	-6 ORFS to -6 STOR	
Valve Pilot Return Hose	–	SAE 100R6-6	
Drain T	–	-6 -8 -6 STOR	
Pressure Reducing Valve Drain Hose	–	SAE 100R6-6	
Valve Line In Hose	–	SAE 100R6-12	
Valve Line In Adapter	–	-12 ORFS -12 STOR	
Spool Valve	–	2 Port Spool Valve	
Outlet Adapter	–	-16 STOR -16 ORFS	
Sch. 40 Pipe	–	7.5 in	
Flow Meter	FLMH-3420SS-MA	3/4" NPTF 20GPM	Omega
Pipe Nipple	–	3/4" - 3/4"	
Needle Valve	N1200S	-12 NPTF -12 NPTF	Parker
Sch. 40 Pipe	–	4 in	
Adapter	–	3/4 NPTF to SAE-16	
Return Hose	–	SAE 100R6-16	
Tee Adapter	–	1" x 3.4" x 3/4"	
Boundary Condition			
Needle Valve BC Hose	–	SAE100R6 -16	
Needle Valve	N1200S	Sch. 40 -12NPTF -12NPTF	Parker
Expansion Chamber BC Hose	–	SAE100R6-16	
Expansion Chamber	–	0.45m -12 NPTF - 16 NPTF	
4 Meter Hose BC Hose	–	SAE100R6-16	
Adapter	–	3/4" NPT to SAE -16	

Table A.1
Spool Valve Configuration Component List

Component	Part Number	Description	Manufacturer
Tachometer	–	Laser Type	
Thermocouple	–	Type K	Omega
Digital Temp. Display	–	Trendicator	Omega
Static Pressure	PX309-5KGV	5000 PSIG MV/V	Omega
Dynamic Pressure	113B22	ICP Piezo Transducer	PCB
LVDT	ACW	± 12.5 mm Range	RDP
LVDT Signal Conditioner	S7AC	Signal Conditioner	RDP
Fitting Adapter	–	-4 STOR -6 STOR	
Accelerometer	–	10 mV/g	PCB

Table A.2
Instrumentation Component List

Appendix B

Additional Figures

The following figures show the time evolution of flow noise on the outlet pressure sensor as the valve is opened. The x axis represents the area at time t normalized by the inlet line cross section. The y axis is the total flow noise divided by the static pressure for that test.

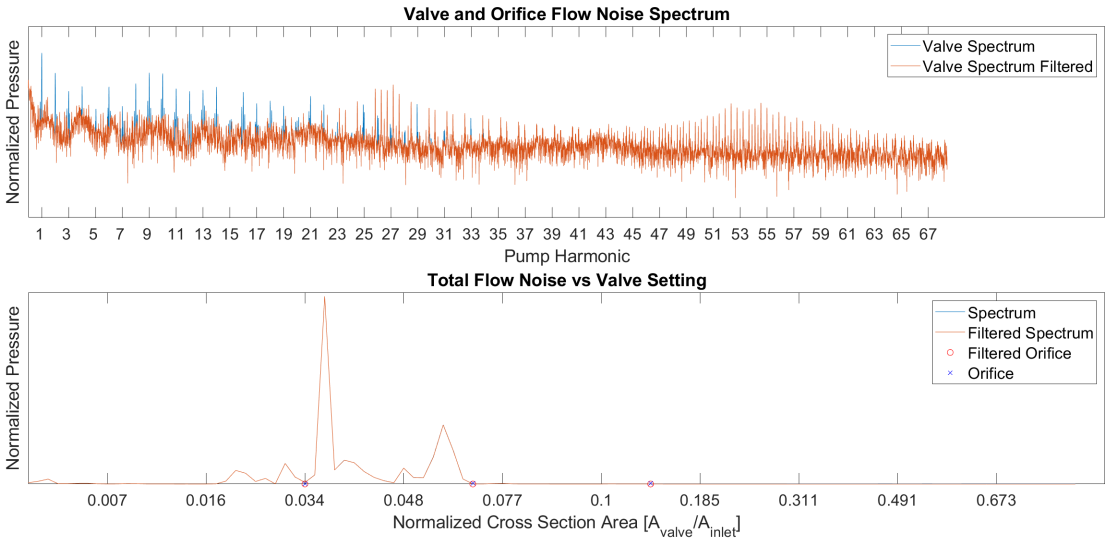

Figure B.1: Flow Noise - Expansion Chamber - 1000 psi 1000 rpm

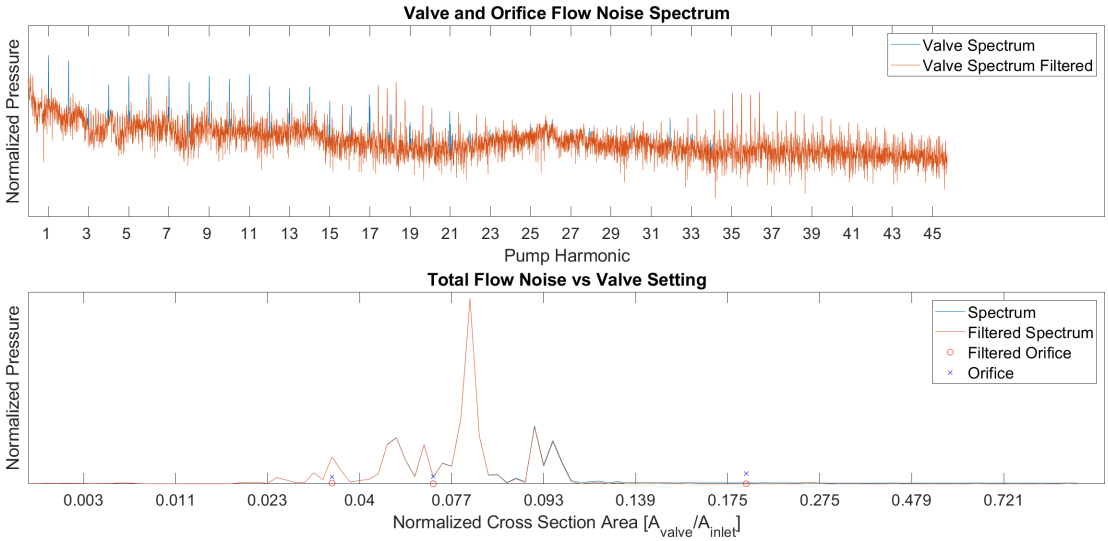

Figure B.2: Flow Noise - Expansion Chamber - 1000 psi 1500 rpm

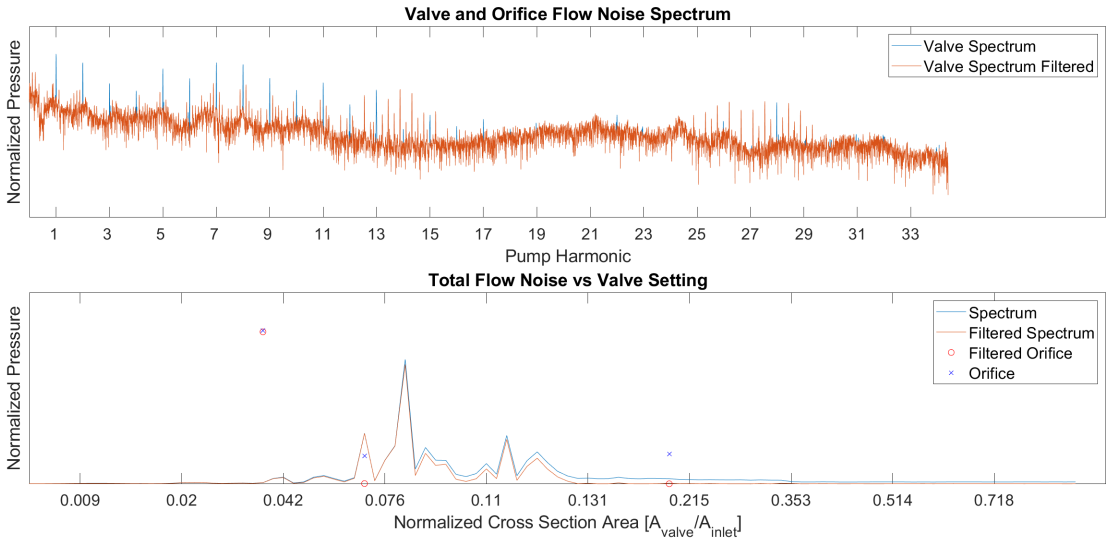

Figure B.3: Flow Noise - Expansion Chamber - 1000 psi 2000 rpm

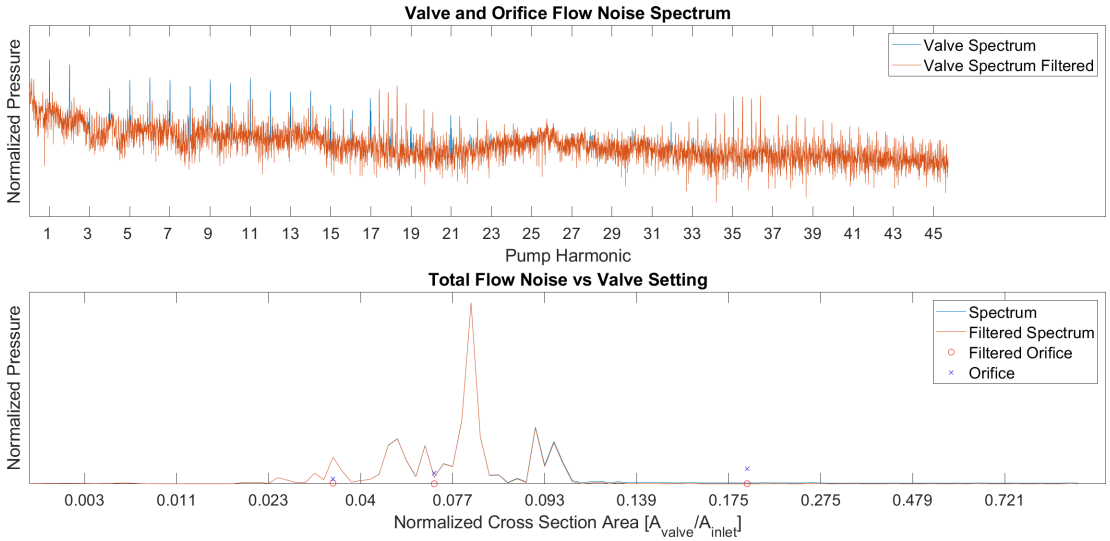

Figure B.4: Flow Noise - Expansion Chamber - 2000 psi 1500 rpm

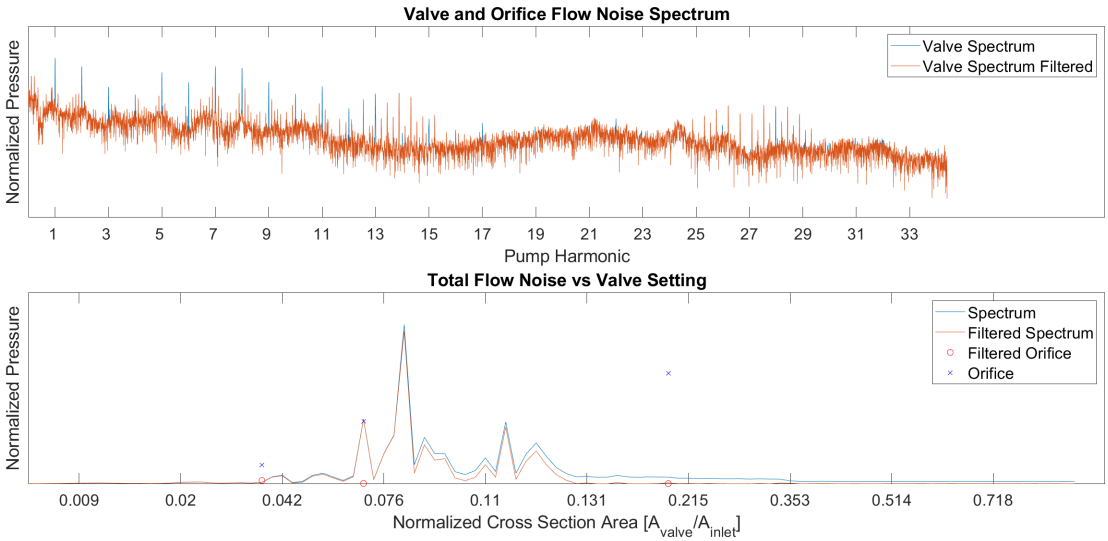

Figure B.5: Flow Noise - Expansion Chamber - 2000 psi 2000 rpm

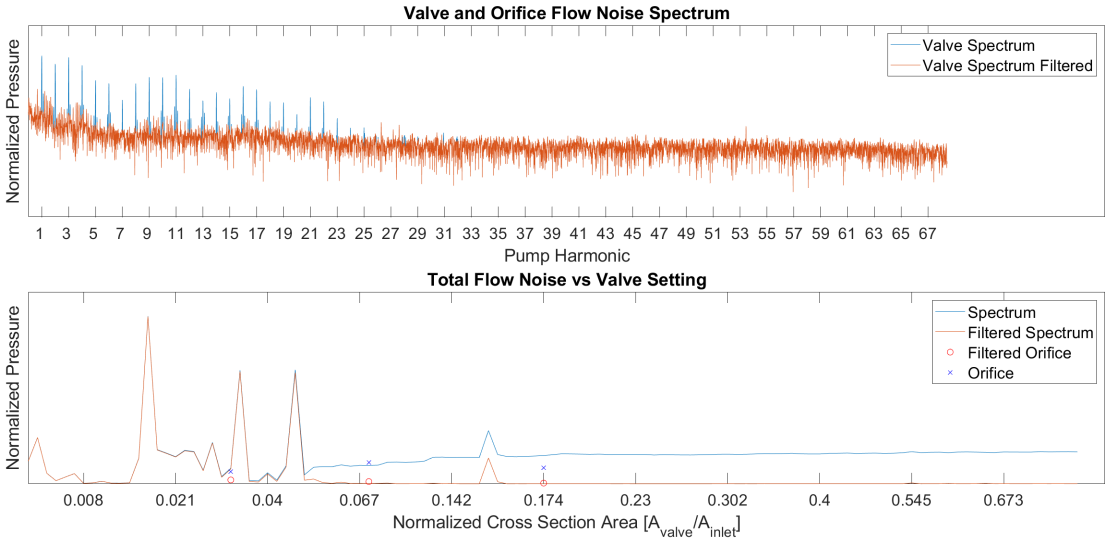

Figure B.6: Flow Noise - 4 Meter Hose - 1000 psi 1000 rpm

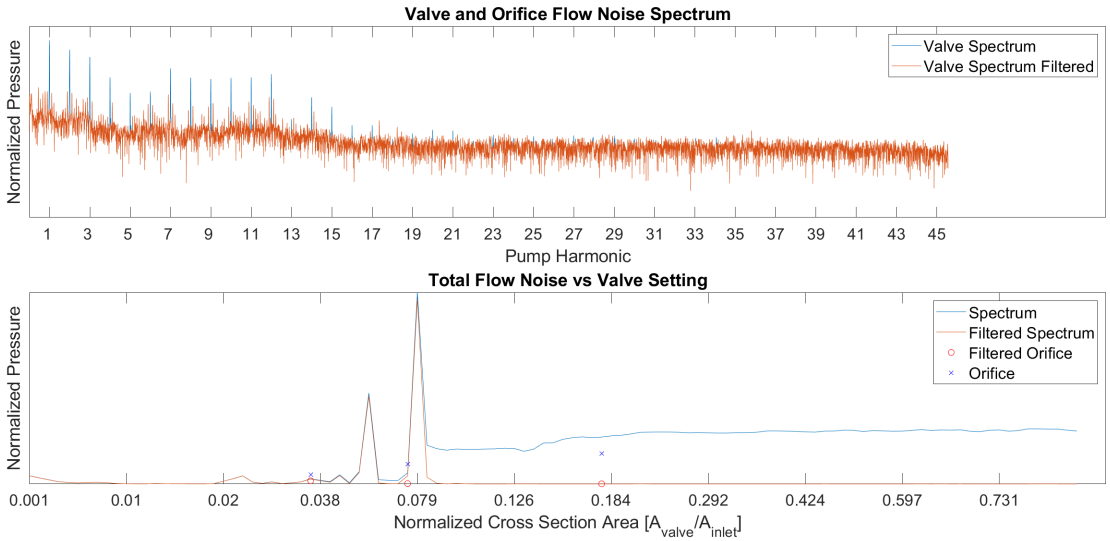

Figure B.7: Flow Noise - 4 Meter Hose - 1000 psi 1500 rpm

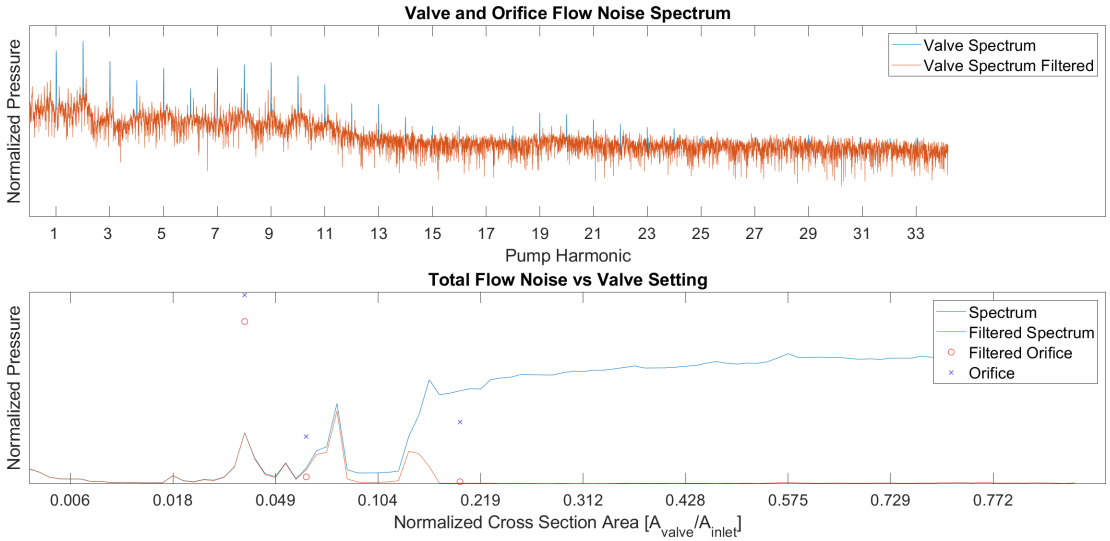

Figure B.8: Flow Noise - 4 Meter Hose - 1000 psi 2000 rpm

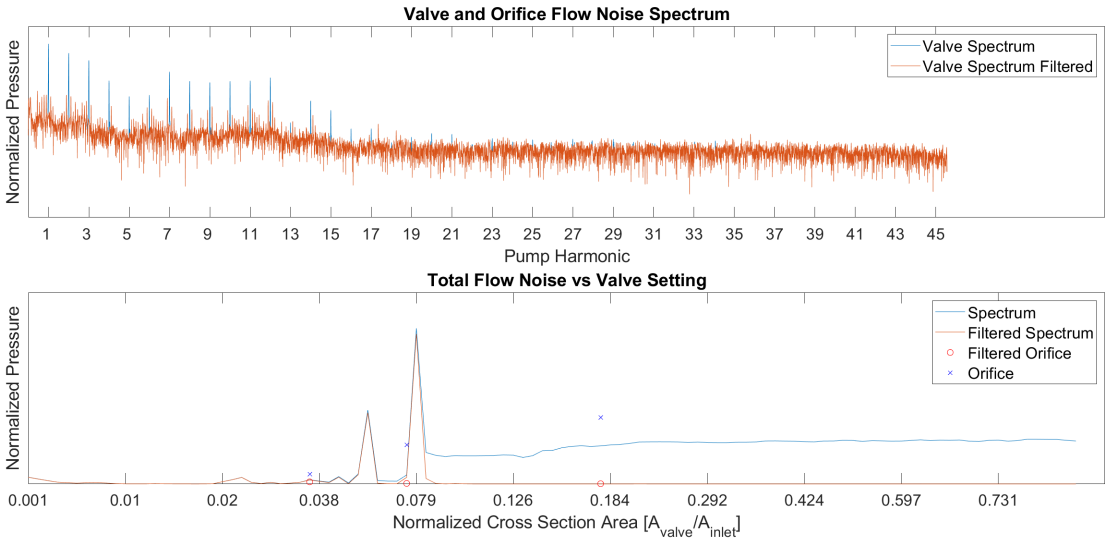

Figure B.9: Flow Noise - 4 Meter Hose - 2000 psi 1500 rpm

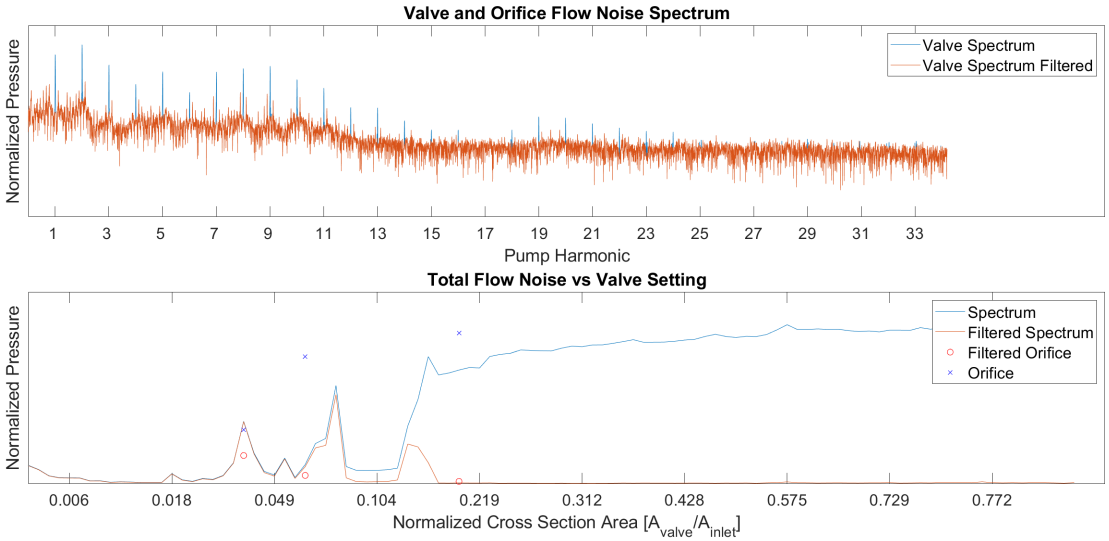

Figure B.10: Flow Noise - 4 Meter Hose - 2000 psi 2000 rpm

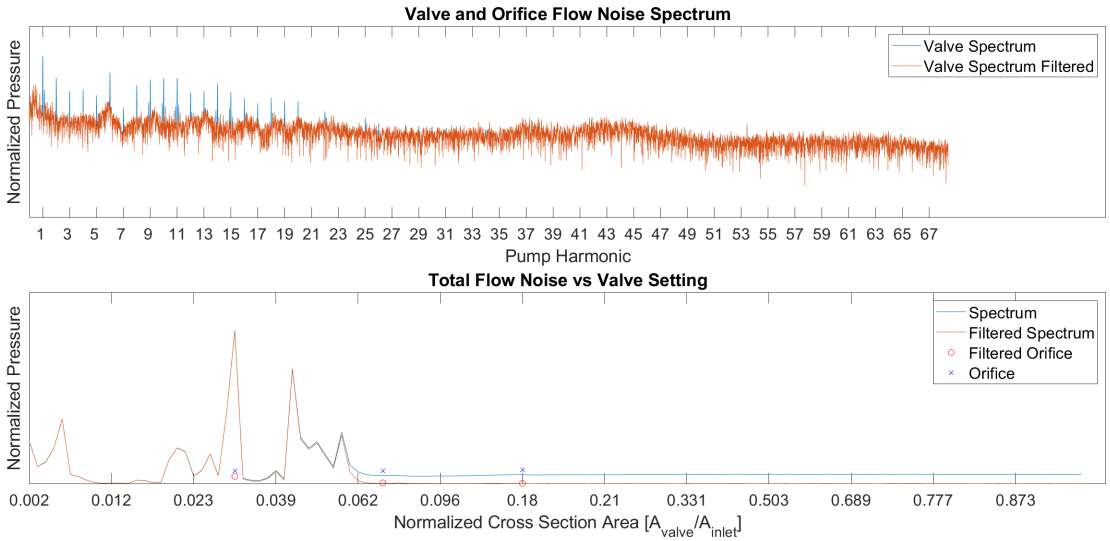

Figure B.11: Flow Noise - Needle Valve - 500 psi 1000 rpm

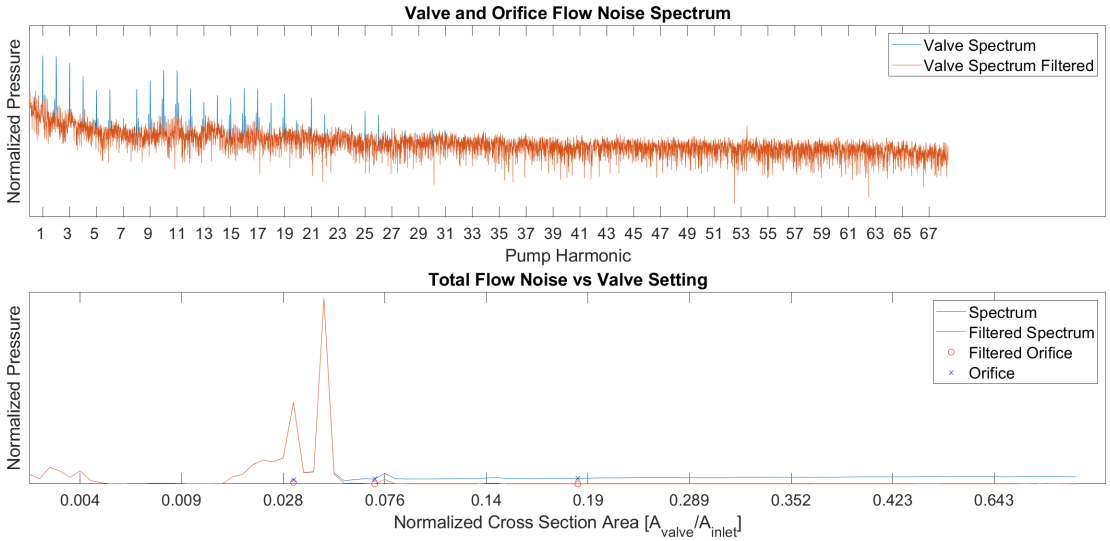

Figure B.12: Flow Noise - Needle Valve - 1000 psi 1000 rpm

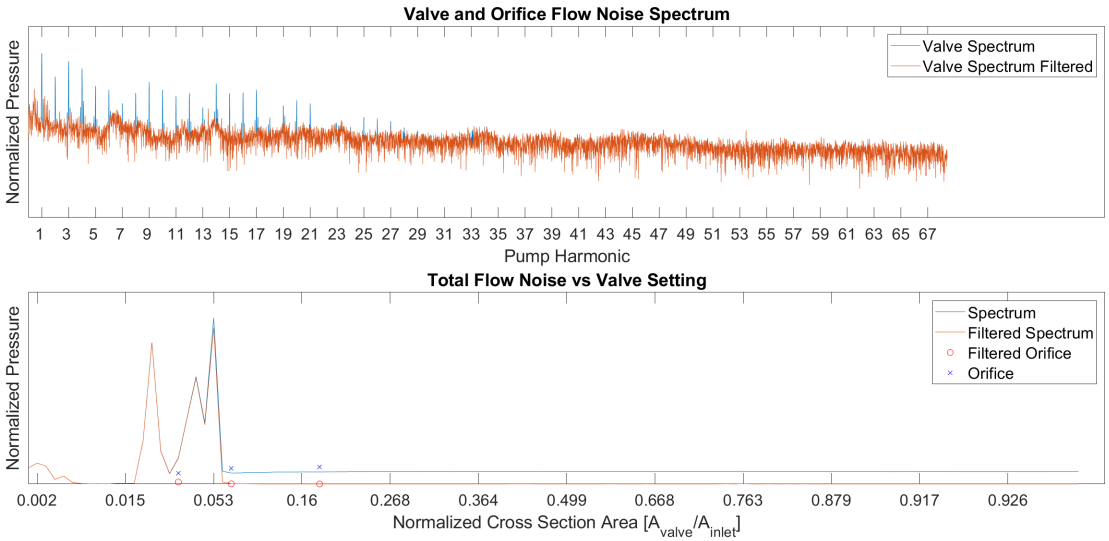

Figure B.13: Flow Noise - Needle Valve - 1500 psi 1000 rpm

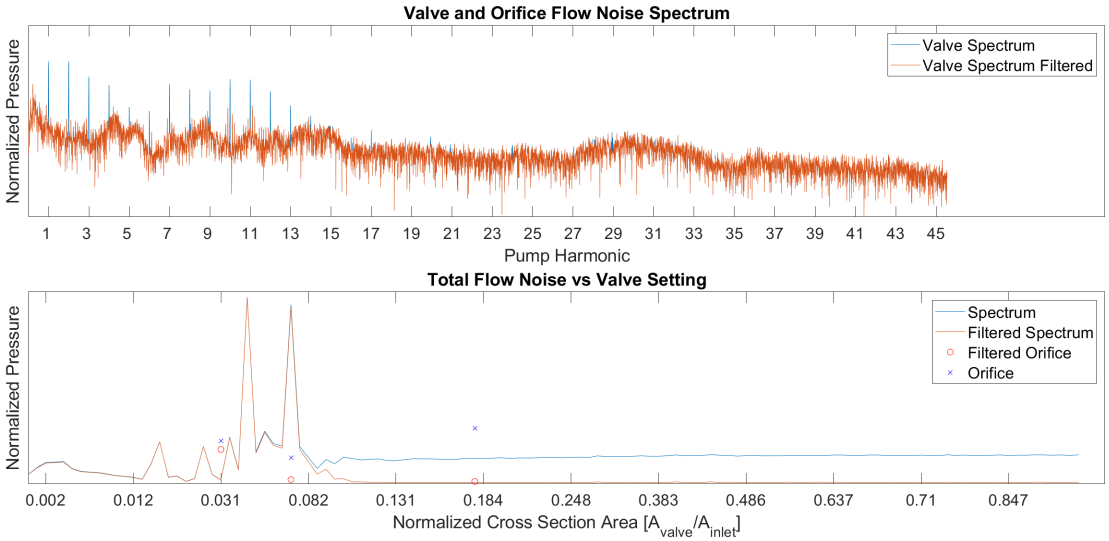

Figure B.14: Flow Noise - Needle Valve - 500 psi 1500 rpm

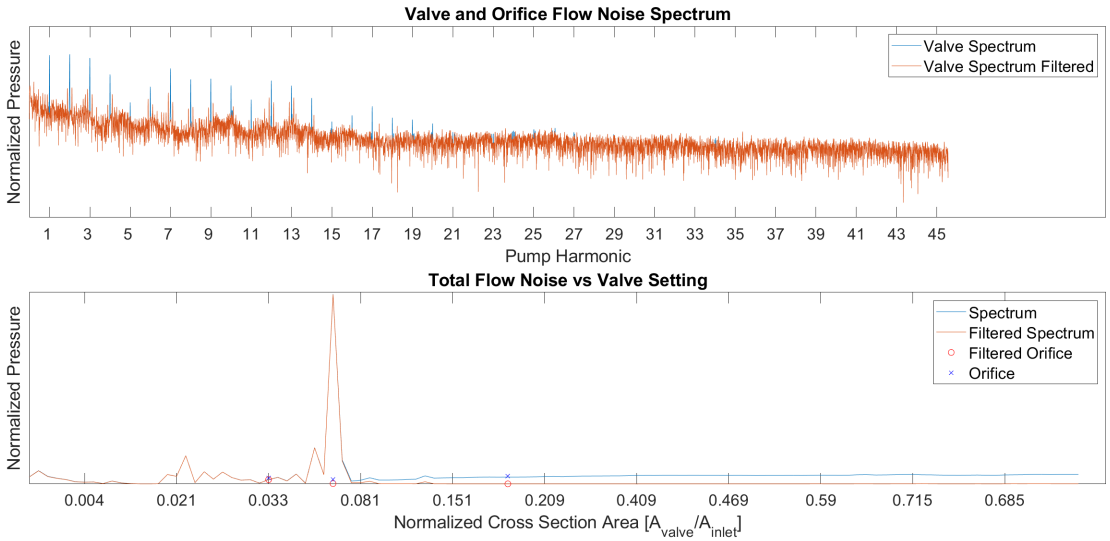

Figure B.15: Flow Noise - Needle Valve - 1000 psi 1500 rpm

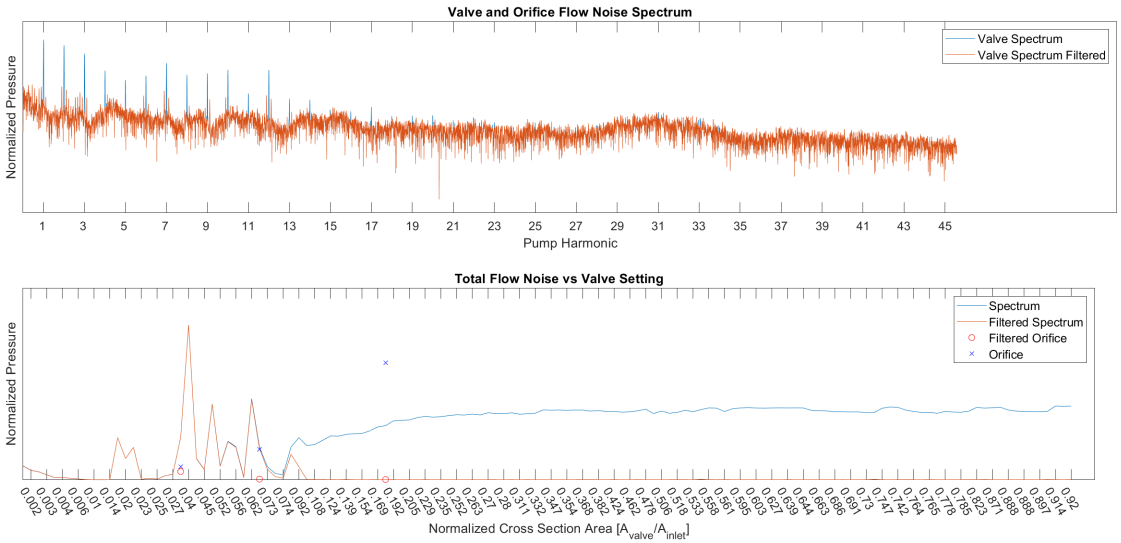

Figure B.16: Flow Noise - Needle Valve - 1500 psi 1500 rpm

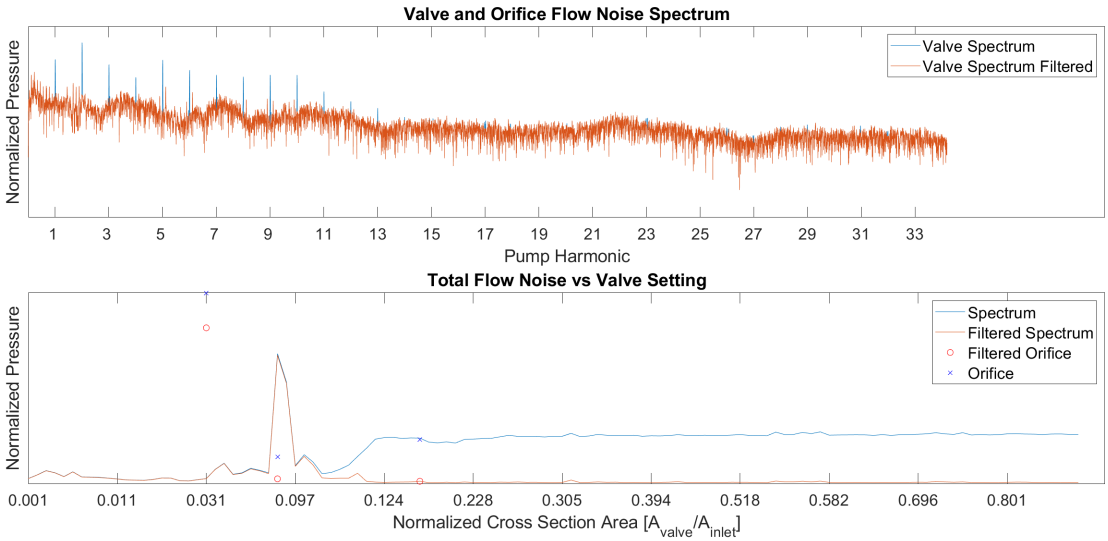

Figure B.17: Flow Noise - Needle Valve - 500 psi 2000 rpm

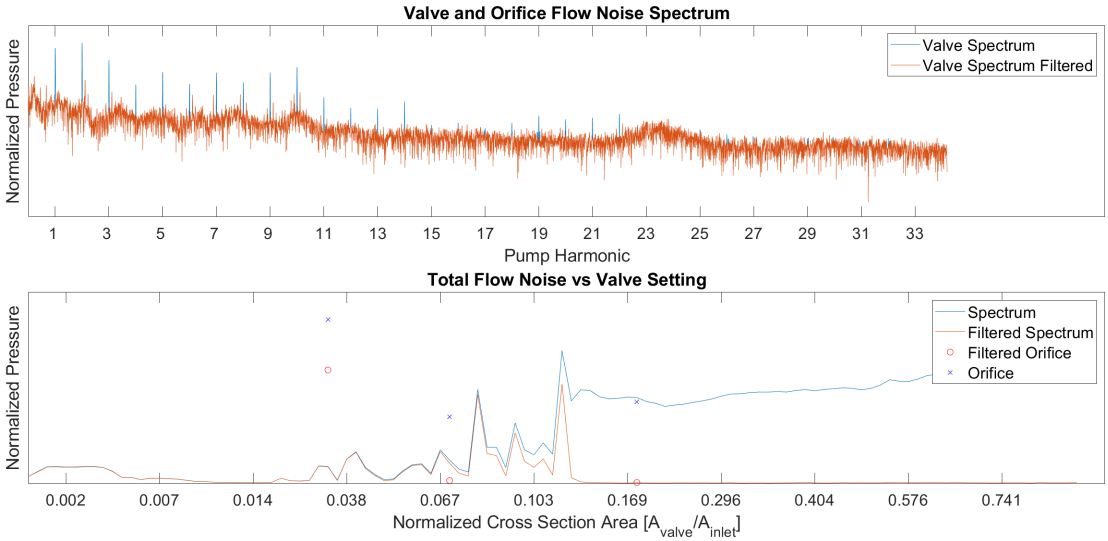

Figure B.18: Flow Noise - Needle Valve - 1000 psi 2000 rpm

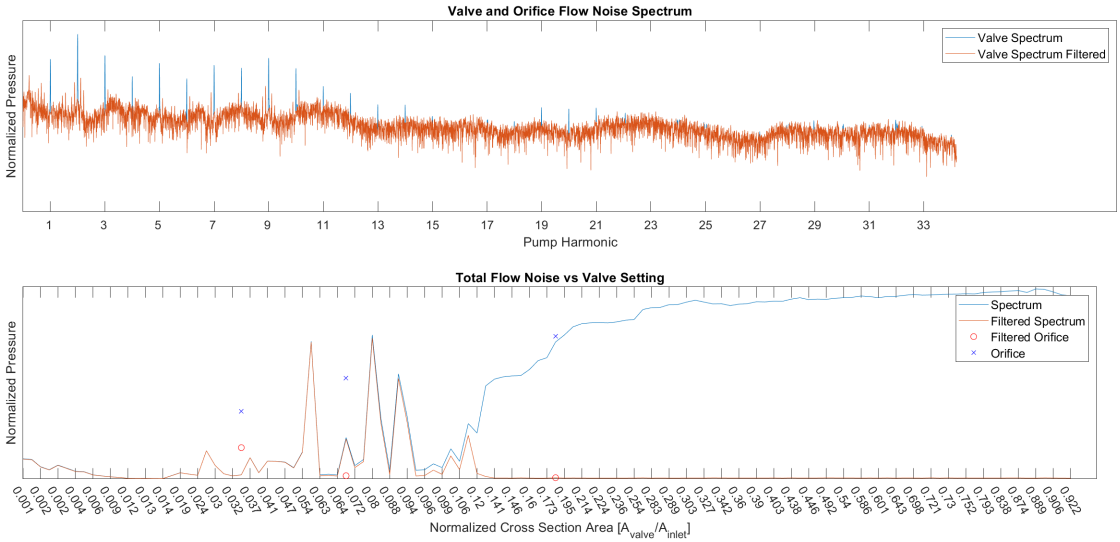

Figure B.19: Flow Noise - Needle Valve - 1500 psi 2000 rpm

Appendix C

Test Bench Startup Procedure

The startup and measurement sequence involves the following:

1. Perform safety inspection and check for oil leaks.

2. Turn on power supplies:

    † Motor power

    † +5 V static pressure sensor supply

    † +5 V LVDT supply

    † +24 V supply for operator controller and flow meter

    † 2 mA current supply for tachometer

3. Open LMS Testlab Signature Testing Advanced. Arm the system in the measurement tab.

4. Run system at 800 rpm for 10 minutes, then increase motor speed to 1000 rpm until oil approaches 50° C. Set desired motor speed.

5. Fully open spool valve. Adjust needle valve to ensure system maintains minimum 500 psi.

6. Perform test.

To test an orifice, follow steps 1 through 4. When oil approaches 50° C ensure desired system pressure is set by adjusting the needle valve, then perform the test.

Appendix D

Removal of Electrical Noise from Dynamic Pressure Sensor Signals

Due to grounding problems on the DAC used in this work, several experiments were affected by electrical noise which was present in the dynamic pressure sensor signals. These signals required filtering and smoothing to remove this electrical noise. Since the dynamic pressure spectra were summed, smoothing the data should not alter the summed spectra significantly. First the spectra were filtered to remove pump harmonics. Above 3500 Hz the spectra were smoothed by a 15th order 1-D median filter. This frequency range was selected based on observation that below 3500 Hz, there was little corruption due to the electrical noise and mainly pump harmonics were present. Since these pump harmonics were previously removed, it was necessary

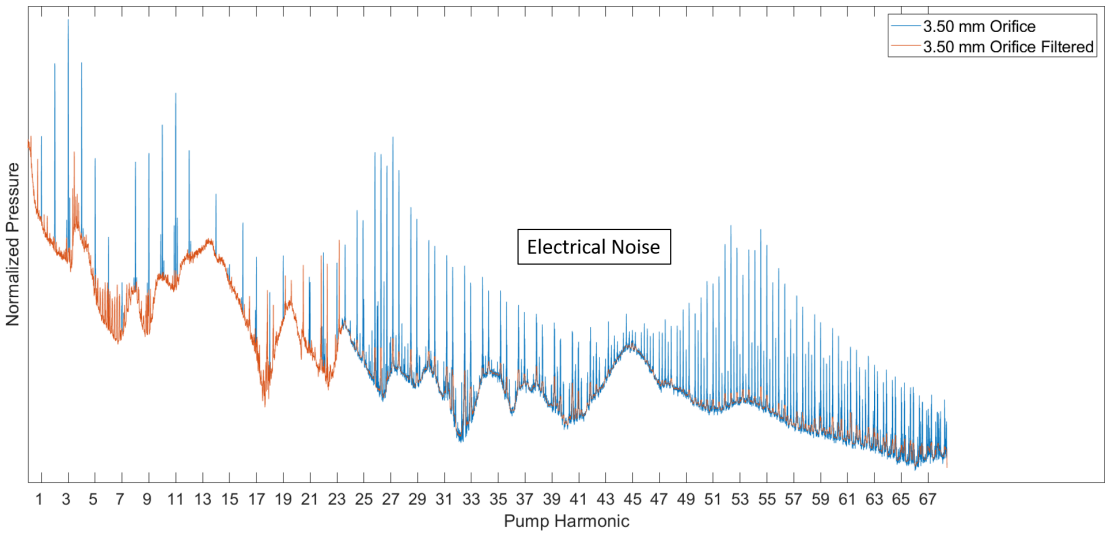

Figure D.1: Electrical Noise Corruption of Dynamic Pressure Sensor Signal and Smoothed Results

to only filter the frequency range above 3500 Hz. Figure D.1 shows the spectra before any processing and again after being filtered and smoothed. The areas with the worst electrical noise are highlighted.